Journal of Pharmacy and Pharmacology, 2025, **00**, 1–22
https://doi.org/10.1093/jpp/rgaf065
Advance access publication 16 August 2025
Review

JPP Journal of Pharmacy and Pharmacology

OXFORD

Icariside II: natural occurrence, biotransformation, pharmacological activity, synthetic modification, pharmacokinetics, and bioavailability

Huynh Thi Ngoc Ni[1], Nguyen Ngoc Linh[2], Phi Thi Tuyet Nhung[2], Pham Thi Bich Dao[2], Vu Quoc Manh[2], Ninh The Son[3,*]

[1]Faculty of Education, Ha Tinh University, Cam Binh, Hatinh 480000, Vietnam
[2]Faculty of Pharmacy, Thanh Do University, Km15 Lai Xa, Hoai Duc, Hanoi 10000, Vietnam
[3]Institute of Chemistry, Vietnam Academy of Science and Technology, 18 Hoang Quoc Viet, Nghia Do, Hanoi 10000, Vietnam

*Corresponding author: Institute of Chemistry, Vietnam Academy of Science and Technology, 18 Hoang Quoc Viet, Caugiay, Hanoi 10000, Vietnam.
Email: ntson@ich.vast.vn and yamantson@gmail.com

Abstract

Objectives: Icariside II (ICS-II), a flavone containing 3-rhamnopyranosyl and 8-prenyl groups, is one of the main natural compounds found in *Epimedum* species (the family Berberidaceae). The current study aims to provide a systematic review of its natural occurrence, pharmacological value, synthetic modification, pharmacokinetics, and bioavailability.

Key findings: Sources such as Google Scholar, Web of Science, PubMed, and journal websites were used to gather references about ICS-II. 'Icariside II' is the most meaningful keyword to seek references, and references have been updated till now.

Summary: ICS-II is a characteristic metabolite of various *Epimedum* plants, and it can be obtained by enzymatic hydrolysis of other flavonoids. It is a promising compound with multiple *in vitro* and *in vivo* pharmacological potentials. The studied flavone showed cancer-related biological activity via cell cycle arrest, proliferation inhibition, autophagy, and apoptosis and inhibited cytokines in anti-inflammatory actions. Significantly, the health benefits were accompanied by its role in antidiabetics, sexual reproduction, and protection against harmful effects on the heart, brain, bones, lungs, kidneys, livers, and eyes. Molecular mechanisms of action were deduced from various signaling pathways, such as Akt/NOS/NF-κB, JAK/STAT3/MAPK, and PI3K/Akt/mTOR. Pharmacokinetic evidence involved sugar and methyl removals, hydroxylation, glucuronidation, and glycosylation.

Keywords: Icariside II; natural occurrence; biotransformation; pharmacological value; pharmacokinetics; bioavailability

Introduction

With their natural origins, plant-based medications and herbal therapies are regarded as safe, and beneficial to health. However, given the growing popularity and usage of plant-based traditional medicines and herbal therapies, it is noted that the understanding of the safety, efficacy, and health implications of these treatments must be addressed [1]. Most medicinal plant materials are collected from wild sources, where a variety of phytochemical ingredients are produced as a result of both extrinsic and intrinsic conditions [2]. Variations in the amounts of physiologically active chemicals in plant material can impact the medication's effectiveness and safety. Furthermore, medicinal plants create secondary metabolites to poison, repel, or even kill dangerous species [3].

Flavonoids are biosynthesized through the phenylpropanoid pathway and contain a C_6-C_3-C_6 carbon skeleton. Flavonoids have been reported as the major dietary constituents of plant-based food. Since they are typically found in significant quantities in the plant kingdom, these phenolic chemicals are found in foods originating from plants [4]. About 4000 chemically distinct flavonoids have been identified and can be divided into several main classes, such as flavones, isoflavones, flavanones, isoflavanones, aurones, chalcones, and anthocyanidins [5]. An estimated less than 80 mg of flavonoids are taken each day [5].

Icariside II (ICS-II) is an 8-prenylated flavonol 3-rhamnopyranoside, which was available in various medicinal plants of the genus *Epimedium*, such as *E. brevicornum*, *E. elatum*, *E. koreanum*, *E. sagittatum*, *E. pubescens*, and *E. wushanense* [6–9]. It was also obtained from other flavones using glycosidic enzymes, especially the hydrolysis of icariin [10–15]. Accumulative reports indicated the great values of ICS-II in pharmacological experiments. For instance, ICS-II showed cancer-related biological activity to cause a cell death program in breast cancer cells via intrinsic and extrinsic signaling pathways [16]. The antidiabetic ability of ICS-II may be attributed to reduce hyperglycemia and hyperlipidemia in mice via reactive oxygen species [17]. ICS-II has been further documented to possess potential effects in protecting the heart, brain, bones, lungs, kidneys, livers, and eyes [18–25].

There are plenty of experimental results, but an overview of its several scientific values has not yet been updated. The current study aims to systematically provide an insightful illustration of the flavone ICS-II's natural occurrence,

Received 27 September 2024; accepted 21 July 2025

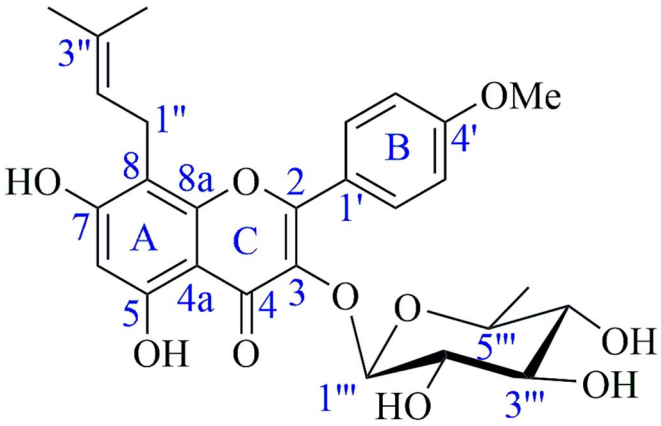

Figure 1. Chemical structure of icariside II.

structural elucidation, biotransformation, pharmacological value, synthetic advance, and pharmacokinetics. Importantly, *in vitro* and *in vivo* molecular mechanisms of action have been reviewed in detail.

Methodology

Data collection was based on various electronic sources, such as Web of Science, PubMed, Google Scholar, and Science Direct. Articles published in English are the main selection. The 'SCI-Finder' was used to confirm the chemical structure. 'Icariside II', '*Epimedium*', 'natural occurrence', and 'pharmacology', are the keywords to search for references, as well as it was used alone or in combination with other meaningful keywords 'biotransformation', 'synthetic modification', 'pharmacokinetics', and 'bioavailability'. Approximately 130 references were collected from the 1990s to the present.

Natural occurrence

In the family Berberidaceae, the genus *Epimedium* contains about 52 herbaceous plants [6–9]. It is recorded that crude extract and isolated compounds from this genus have various pharmacological values, such as cancer-related biological activity, anti-inflammation, and organ protection [6–9]. Evidence from phytochemical investigations indicated that flavonoids containing prenyl units were the primary naturally occurring metabolites, especially two natural products icaritin and ICS-II (Fig. 1). ICS-II was classified as an 8-prenylated flavonol glycoside, which was detectable in numerous *Epimedium* species. As an example, this molecule has been observed in Korean *E. koreanum* aerial parts [18]. Using high-speed counter-current chromatography (HSCCC) and a mobile phase of CH_2Cl_2–MeOH-H_2O (4,3.5,2, v/v/v), ICS-II was also isolated from Chinese *E. koreanum* aerial parts in one step with a purity of 99.7% [6]. ICS-II was present in *E. brevicornum*, one of the ingredients of traditional Chinese medicine Xian-Ling-Gu-Bao [26]. The contents of ICS-II in Herba Epimedii studied batches were estimated as *E. brevicornum* (0.22–2.59 mg/g), *E. sagittatum* (1.59–10.23 mg/g), *E. koreanum* (1.01–6.20 mg/g), *E. pubescens* (1.97–4.53 mg/g), and *E. wushanense* (1.94–6.90 mg/g) [7]. In another study, ICS-II accounted for 0.001–0.007% of dry weight in the aerial and underground parts of *E. elatum* [8]. It is also concluded that the ICS-II percentages in wild *E. elatum* species are always higher than those in cultivated *E. elatum* [9].

ICS-II was obtained as green-yellow needle crystals with a molecular formula $C_{27}H_{30}O_{10}$ (ESIMS, *m/z*: 515 $[M+H]^+$) and m.p. 205–207°C [10]. Its UV (λ_{nm} (logε)) spectrum included absorbances at 223 (sh, 4.28), 271 (4.31), 300 (3.84), and 350 (3.80) nm, whereas the broad peak at 3420 cm^{-1} in the FT-IR spectrum indicated the presence of OH groups [10]. The ^1H and ^{13}C-NMR spectral data from Table S1 revealed that ICS-II was an 8-prenylated flavonol 3-rhamnopyranose [10].

Biotransformation

By removing excess sugar residues, flavonoid glycosides can be transformed into other derivatives with stronger activity. Among them, α-L-rhamnosidase, with high specificity on α-1, 6- or α-1,2-rhamnosidase, and β-glucosidase, could transform epimedin C into, icariin, icaritin, sagittatoside C, and icariside I, especially in terms of ICS-II (Fig. 2). Epimedin C (5 g/L) was converted into ICS-II (3.122 g/L) via two steps with 1 h incubation under pH 6.5 at 40°C after addition of 5.5 U/mL α-L-rhamnosidase PodoRha (which derived from *Paenibacillus odorifer*); then with 30 min incubation under pH 6.5 at 90°C after addition of 0.8 U/mL β-D-glucosidase IagBgl1 [14].

β-Glucosidase enzyme could convert icariin (200 mg) into ICS-II (95.5 mg, 99.1% purity) under the optimal conditions: 50°C, 0.2 M disodium hydrogen phosphate, citric acid buffer system (pH 6.0), 1:1 icariin/enzyme ratio during the 5-hour reaction period [10]. Radiating the blue light on *E. sagittatum* species upregulated the ICS-II synthesis better than using the red and yellow lights, in which the blue light treatment increased the content of ICS-II up to 66.12% after 30 days of treatment [15]. Using β-glucosidase from *Trichoderma viride* would help to increase the conversion rate of ISC-II from icariin up to 95.03% at 1 h.[12] ICS-II was obtained by hydrolysis of the 7-glycosyl unit of icariin using the fungi *Cunninghamella blakesleana* and *Hormoconis resinae* in yields of 95.1% and 98%, respectively [11, 13].

Pharmacological activities

Cancer-related biological activity

ICS-II at 10 μM was cytotoxic towards five cancer cell lines HL-60, K562, PG, KB, and BGC with inhibitory percentages

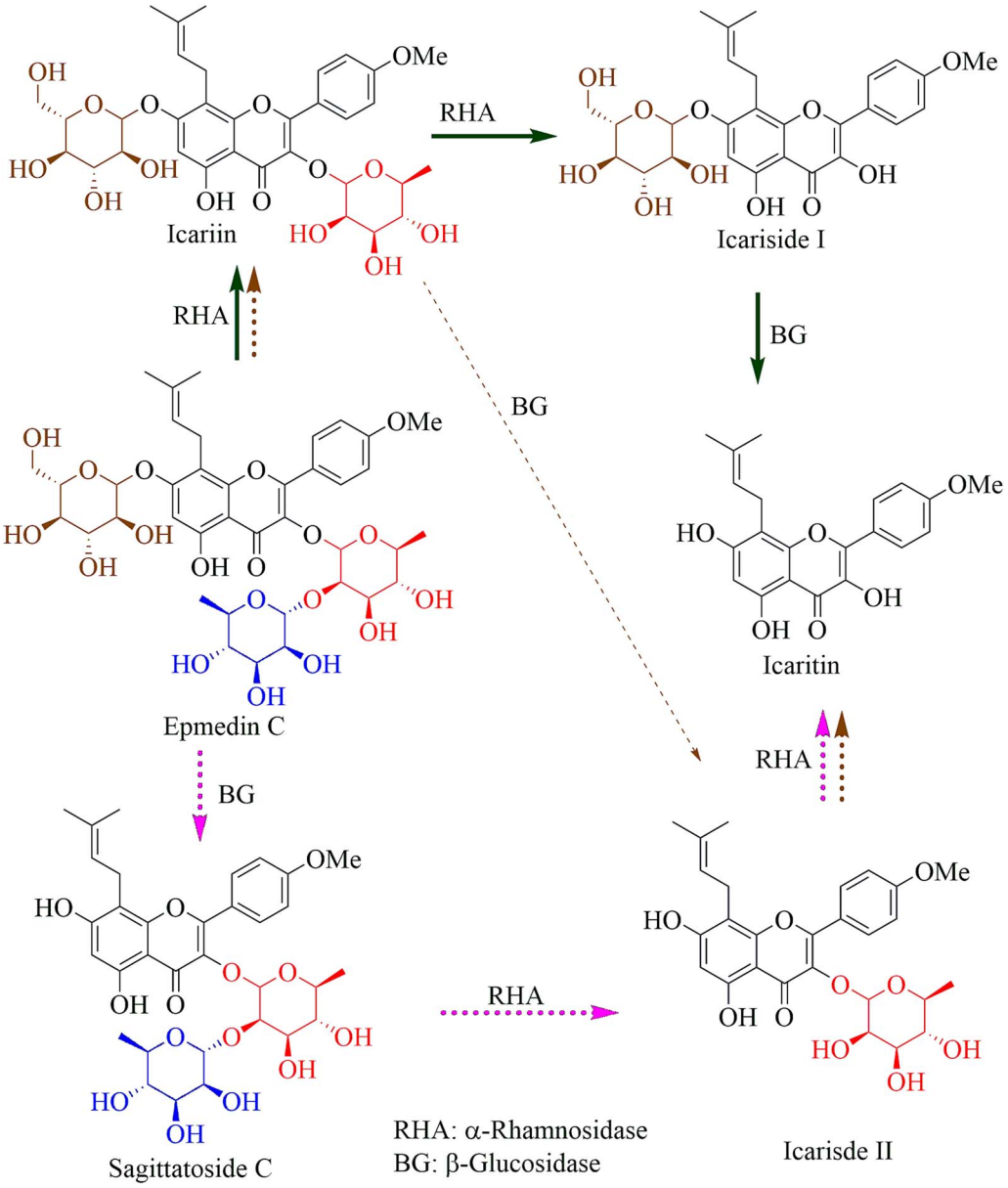

Figure 2. Biotransformation of icariside II.

of 53–88% [27]. At 25–100 μM, ICS-II induced apoptosis in U937 acute myeloid leukemia cells, deducing from the signal transducer and activator of transcription 3 (STAT3) inactivation (activations of caspase 3 and cleaved poly (ADP-ribose) polymerase (PARP), downregulations of Bcl-x_L and survivin, Janus activated kinase 2 (JAK2) suppression, and enhancement of protein tyrosine phosphatase (PTP) SH2 domain-containing phosphatase (SHP)-1) [28]. Similarly, ICS-II could induce apoptosis in U266 multiple myeloma cells via STAT3 inhibition by suppressing JAK2 and c-Src, downregulating Bcl-2, Bcl-x_L, survivin, cyclin D_1, cyclooxygenase-2 (COX-2), and vascular endothelial growth factor (VEGF), but enhancing PARP cleavage and caspase-3 activation [29]. Yang et al. also revealed that ICS-II induced cell cycle arrest and differentiation via toll-like receptor 8 (TLR8)/myeloid differentiation factor 88 (MyD88)/p38 pathway in acute myeloid leukemia cells [30]. This is caused by down-regulating cyclin-dependent kinases (CDK2, CDK4, and CDK6) and up-regulating cyclin-dependent kinase inhibitors (p21 and p27) (Table 1) [30].

At the optimal concentration of 50 μM, ICS-II caused apoptosis in HSC-4 human oral squamous cancer cells via activating ICAD, PARP, and caspase 3, 9 [31]. ICS-II (25–75 μM) caused apoptosis in MCF7 breast cancer cells via intrinsic and extrinsic signaling pathways [16]. The intrinsic actions related to the loss of mitochondrial membrane potential and release of cytochrome *c* and apoptosis-induced factor (AIF), and caspase 9 activation, whereas the extrinsic way was due to Fas/FADD (Fas-associated death domain) enhancement and caspase 8 activation (Fig. 3). The intravenous injection of TPGS (D-α-tocopheryl polyethylene glycol 1000 succinate)-ICS-II-phospholipid micelles (10 mg/kg) to mice bearing MCF7 cells resulted in better cancer-related biological effects, compared with that of free ISC-II, without

Table 1. Pharmacological activities of icariside II.

Models	Concentrations	Effects/mechanisms	References
Cancer-related biological activity			
In vitro	10 μM	53.89% Inhibition/PG 56.6% Inhibition/HL-60 70.37% Inhibition/BGC 73.19% Inhibition/K562 88.61% Inhibition/KB	[27]
In vitro	25–100 μM	Apoptosis in U937 and U266 cells via STAT3 inactivation	[28, 29]
In vitro	10–40 μM	Cycle arrest and differentiation in HL-60 and THP-1 cells via TLR8/MyD88/p38 signaling pathway	[30]
In vitro	50 μM	Apoptosis in HSC-4 cells via activating ICAD, PARP, and caspase 3, 9	[31]
In vitro	25–75 μM	Apoptosis in MCF7 breast cancer cells via intrinsic and extrinsic signaling pathways	[16]
In vivo	TPGS-ICS-II-phospholipid micelles (10 mg/kg, i.v.)	Apoptosis in mice bearing MCF7 cells via Bax/Bcl-2 regulation, and caspase-3, 8, 9 activation	[32]
In vivo	ICS-II (20–40 mg/kg, i.g.) + anti-PD-1 (200 μ/mouse)	To inhibit the tumor growth in mice bearing LLC cells via ROS-mediated inactivation of SRC/ERK/STAT3 signaling pathway	[33]
In vivo	ICS-II (10 mg/kg, p.o.) + cisplatin (3 mg/kg, p.o.)	Apoptosis in mice bearing LLC cells via PERK/eIF2α/ATF4/CHOP signaling pathway	[34]
In vitro	10–20 μM	To inhibit EMT of A549 cells via Akt/NF-κB signaling downregulation	[35]
In vivo	30–60 mg/kg, i.p.	To inhibit EMT of mice bearing A549 cells via Akt/NF-κB signaling downregulation	[35]
In vitro	5–40 μM	Apoptosis in PC-3 cells by inhibiting COX-2/PGE2 via mitochondrial pathway	[36]
In vitro	10–20 μM	To disrupt abnormal energy homeostasis in S180 cells via mTORC1/4E/BP1 axis suppression	[37]
In vivo	10–30 mg/kg, i.p.	To disrupt abnormal energy homeostasis in mice bearing S180 cells via mTORC1/4E/BP1 axis suppression	[37]
In vitro	40–60 μM	Autophagy in SKOV3 and A2780 cells via miR-144-3p/IGF2R axis	[38]
In vivo	25 mg/kg, i.g.	Autophagy in mice bearing A2780 cells via miR-144-3p/IGF2R axis	[38]
In vitro	10–40 μM	Ferroptosis in ACHN and Caki-1 cells via miR-324-3p/GPX4 axis regulation	[39]
In vivo	15–35 mg/kg, i.v.	Ferroptosis in mice bearing ACHN and Caki-1 cells via miR-324-3p/GPX4 axis regulation	[39]
In vitro	5–10 μM	To enhance antioxidant effects in HepG2 cells via Nrf2/ARE signaling regulation	[40]
In vitro	20–30 μM	Apoptosis in HepG2 cells via mitochondrial and lysosomal damages	[41]
In vivo	20–30 mg/kg, i.v.	Apoptosis in mice bearing HepG2 cells via mitochondrial and lysosomal damages	[41]
In vitro	20–40 μM	Apoptosis in DU145 cancer cells via PI3K/Akt/mTOR signaling pathway	[42]
In vitro	15 μM	To suppress tumorigenesis in SW620 cancer cells via circβ-catenin-Wnt/β-catenin axis regulation	[43]
In vivo	25 mg/kg, i.p.	To suppress tumorigenesis in mice bearing SW620 cancer cells via circβ-catenin-Wnt/β-catenin axis regulation	[43]
In vitro	20–40 mM	Apoptosis in U87 and A172 cells via inhibiting Akt and potentiating FOXO3a	[44]
In vitro	5–30 μM	To inhibit HeLa cells via JNK/MMP-2/9 signaling inhibition	[45]
In vivo	25 mg/kg, i.v.	To inhibit mice bearing HeLa cells via JNK/MMP-2/9 signaling inhibition	[45]
In vitro	20–30 μM	To reduce the proliferation of MG-63 and Saos-2 cells via EGFR/mTOR signaling activation	[47]
In vivo	10–30 mg/kg, i.p.	To reduce the proliferation of mice bearing sarcoma-180 via EGFR/mTOR signaling activation	[47]
In vitro	50 μM	Apoptosis in A431 cells via EGFR signaling inhibition	[48]
In vitro	20 μM	To improve ROS generation, induce ROS-dependent apoptosis and autophagy, and downregulate MITF expression in A2058 and A375R cells	[49]
In vitro	25–100 μM	To inhibit proliferation and induce cell cycle arrest in A375 cells via ROS-p38-p35 signaling pathway	[50]
In vitro	ICS-II (10 μM) + paclitaxel (10 nM)	Apoptosis in A375 cells via TLR4/MyD88/ERK signaling pathway	[51]
In vitro	ICS-II (20 μM) + TRAIL (25 ng/mL)	Apoptosis in A375 cells via ROS-mediated downregulation of STAT3/cFLIP signaling pathway	[52]
In vivo	50 mg/kg, i.p.	Apoptosis in mice bearing A375 cells via JAK/STAT3/MAPK signaling downregulation	[53]
Anti-inflammatory activity			
In vivo	3–10 mg/kg, i.p.	To attenuate LPS-mediated neuroinflammation in mice via TLR4/MyD88/NF-κB signaling inhibition	[54]
In vitro	5–20 μM	To inhibit LPS-induced inflammation in rat astrocytes by IKK/IκB/NF-κB/BACE1 signaling regulation	[55]
In vitro	1.0 μM	eNOS-Ser1177 phosphorylation in HUVECs via PI3K/Akt, AMPK and PKC signaling pathways	[56]
In vivo	10–30 mg/kg, i.p.	To attenuate eosinophils-induced airway inflammation and remodeling in mice via NF-κB/STAT3 signaling inactivation	[57]
Antidiabetic activity			
In vitro		$IC_{50} = 106.59$ μM/α-glucosidase	[58]
In vivo	5 mg/kg, p.o.	To inhibit STZ-induced diabetic mice via TGF-β/Smad/CTGF signaling downregulation	[59]

(continued)

Table 1. Continued.

Models	Concentrations	Effects/mechanisms	References
In vivo	10–40 mg/kg, i.g.	To diminish hyperglycemia and hyperlipidemia in mice by targeting PPARα/γ via ROS/NF-κB/IRS1 signaling pathway	[17]
In vivo	5 mg/kg, i.p.	To improve diabetic cardiomyopathy in STZ-stimulated diabetic mice via Akt/NOS/NF-κB signaling activation	[60]
In vitro	0.01–1.0 μM	To inhibit high glucose-mediated damages in HCECs via Akt/eNOS signaling pathway	[61]
In vitro	0.1–10 μM	To ameliorate endothelial dysfunction in HCECs via miR-126/SPRED1 signaling pathway	[62]
Aphrodisiac activity			
In vivo	5 mg/kg, i.p.	To impair the corpus cavernosum and major pelvic ganglion neuropathy in STZ-induced diabetic mice	[63]
In vivo	1–10 mg/kg, p.o.	To alter the corpus cavernosum fibrous-muscular pathological structure in diabetic mice via TGFβ1/Smad2/CTGF and NO-cGMP signaling regulations	[64]
In vivo	ICS-II (10 mg/kg, i.g.) + metformin (0.2 g/kg, i.p.)	To improve penile erectile dysfunction in T2DMED mice via PI3K/Akt/mTOR signaling pathway	[65, 66]
In vivo	ICS-II (5 mg/kg, i.p.) + (2–6 units)	To restore erectile function in STZ-mediated T1D rats via AGEs/RAGE oxidative stress axis downregulation	[67]
In vitro	10–40 μM	To decrease testosterone production in rat Leydig cells by depleting NAD^+ and ATP levels via necrosis	[68]
In vitro	0.01–10 μM	To promote the differentiation of ADSCs to SCs via miR-33/GDNF axis regulation	[69, 70]
In vivo	4.5 mg/kg, i.g.	To restore ED in mice via miR-33/GDNF axis regulation	[69, 70]
In vivo	1.5 mg/kg	To inhibit obesity-associated ED in mice via endogenous progenitor cell preservation and proliferation	[71]
Cardiovascular activity			
In vivo	4–16 mg/kg, i.g.	To attenuate myocardial fibrosis in mice via inhibiting NF-κB and TGF-β1/Smad2 signaling pathways	[20]
In vivo	8–16 mg/kg, i.g.	To attenuate myocardial fibrosis in mice by inhibiting collagen synthesis via MMP/TIMP-1 and TGF-β1/Smad2,3/p-p38 signaling pathways	[21]
In vitro	1–5 μM	To attenuate palmitic acid-mediated endothelial dysfunction via SRPK1/Akt/eNOS signaling pathway	[72]
In vivo	20 mg/kg, i.g.	To restore the VSMC contractile phenotype by enhancing the focal adhesion in the rat vascular remodeling model	[73]
In vitro	20 μM	To attenuate cardiac hypertrophy in H9C2 cells via sirtuin/AMPK signaling activation	[75]
In vivo	16 mg/kg, i.g.	To attenuate cardiac hypertrophy in mice via sirtuin/AMPK signaling activation	[75]
In vitro	2–8 μM	To inhibit hypoxia-mediated H9C2 cells via PI3K/Akt signaling pathway	[76]
In vitro	20 μM	To attenuate cardiac remodeling in neonatal rat cardiomyocytes via AMPKα2/mTORC1 signaling pathway	[77]
In vivo	10 mg/kg, i.g.	To attenuate cardiac remodeling in mice via AMPKα2/mTORC1 signaling pathway	[77]
In vivo	4–16 mg/kg, i.g.	To prevent hypertensive heart disease via PERK/ATF-4/CHOP signaling pathway in hypertensive mice	[78]
In vitro	2–8 μM	To protect against myocardial infarction in H9C2 cells via AMPK/PGC-1α/apoptosis signaling pathway	[79]
In vivo	5–20 mg/kg, i.p.	To protect against myocardial infarction in mice via AMPK/PGC-1α/apoptosis signaling pathway	[79]
In vitro	20 μM	To protect against myocardial infarction in H9C2 cells via Nrf2/SIRT3 signaling activation	[80]
In vivo	20 mg/kg, i.p.	To protect against myocardial infarction in mice via Nrf2/SIRT3 signaling activation	[80]
Brain protective activity			
In vitro		$IC_{50} = 13.29$ μM/dopamine D3 receptor	[22]
In vitro	3–10 μM	To differentiate human amniotic mesenchymal stem cells into dopaminergic neuron-like cells via PI3K signaling pathway	[81]
In vivo	10–30 mg/kg, p.o.	To attenuate methamphetamine-induced neurotoxicity and behavioral impairments in mice via Keap1/Nrf2 signaling activation	[82]
In vitro	10 μM	To alleviate inflammatory and neuropathic pain in tsA-2011 cells by suppressing T-type calcium channels and USP5-Cav3.2 interactions	[83]
In vivo	20 mg/kg, i.p.	To reverse Aβ-mediated cognitive impairment in mice via inflammatory and apoptotic reductions	[84]
In vivo	8–16 mg/kg, i.g.	To ameliorate ibotenic acid-mediated cognitive impairment and apoptotic response through MAPK modulation in mice	[85]
In vivo	20 mg/kg, p.o.	To alleviate cerebral microcirculatory disturbance and improve hippocampal damage in I/R mice	[86]
In vivo	10–30 mg/kg, p.o.	To reduce spatial learning and memory impairments in AD mice via Aβ production	[87]
In vivo	16 mg/kg, p.o.	To ameliorate cognitive impairments in CCH-mediated mice via BDNF/TrkB/CREB signaling pathway	[88]
In vivo	8 mg/kg, i.p.	To promote hippocampal neuron axon regeneration and improve learning and memory in CCH mice	[89]
In vivo	5–20 mg/kg, p.o.	To protect against ischemic stroke via the astrocytic Nrf2-mediated OXPHOS/NF-κB/ferroptosis axis	[90]
In vivo	4–16 mg/kg, i.g.	To attenuate cerebral I/R-mediated damage in mice via PKG/GSK-3β/autophagy axis inhibition	[91]

(continued)

Table 1. Continued.

Models	Concentrations	Effects/mechanisms	References
In vivo	20 mg/kg, i.g.	To attenuate cerebral I/R-mediated damage in mice via oxidative stress reduction and Nrf2/HO-1 expression improvement	[92]
In vivo	10–30 mg/kg, i.p.	To protect against cerebral I/R damage in MCAO mice via up-regulation of PPARα and PPARγ and NF-κB suppression	[93]
In vivo	16 mg/kg, i.p.	To attenuate I/R-induced blood–brain barrier dysfunction in mice via MMP9/TIMP1 balance regulation	[94]
In vivo	1–10 mg/kg, i.g.	To alleviate chronic hydrocephalus in SAH mice via TGF-β1/Smad/CTGF signaling regulation	[95]
In vitro	25–100 μM	To inhibit H_2O_2-induced PC12 cells death via ROS/GSK-3β/mitochondrial signaling pathway	[96]
In vitro	25–100 μM	To promote neuron-like PC12 cell growth via Akt/nNOS/NO/cGMP/PKG activations	[97]
In vitro	12.5–50 μM	To alleviate OGD/R-mediated PC12 cells oxidative damages via Nrf2/SIRT3 signaling activation	[98]
In vitro	12.5–50 μM	To rescue OGD/R-mediated hippocampal neuronal injury via PDEE5 inhibition and PKG/CREB/BDNF/TrkB signaling activation	[99]
In vitro	25 μM	To attenuate Aβ_{25-35}-mediated cognitive deficits in PC12 cells via CREB/BDNF/TrkB signaling pathway	[100]
In vivo	10 mg/kg, i.g.	To attenuate Aβ_{25-35}-mediated cognitive deficits in mice via CREB/BDNF/TrkB signaling pathway	[100]
In vivo	10 mg/kg, i.g.	To suppress STZ-mediated cognitive deficits in mice	[101]
In vitro	12.5–50 μM	To suppresses ferroptosis to protect against MPP^+-induced PD in SK-N-SH cells through Keap1/Nrf2/GPX4 signaling pathway	[102]
In vitro	12.5–50 μM	To protect dopaminergic neurons in SK-N-SH cells by downregulating HDAC2 to restore mitochondrial function	[103]
Bone protective activity			
In vitro	10 μM	To improve osteogenic differentiation of BMSCs	[19]
In vitro	10^{-9}–10^{-5} mol/L	To promote osteogenic differentiation of canine bone marrow mesenchymal stem cells via PI3K/AKT/mTOR/S6K1 and MAPK/ERK signaling pathways	[104, 105]
In vitro	0.01–10 μM	To stimulate osteogenesis, and inhibit adipogenesis in MSCs via ERK signaling pathway	[106]
In vitro	20 ng/dL	To enhance the growth and differentiation of osteoblast and osteoprotegerin expression	[107]
In vitro	5 μM	To diminish dexamethasone-elicited apoptosis in MC3T3-E1 cells via EGFR/Akt/Nrf2 signaling pathway	[108]
In vivo	10–20 mg/kg, p.o.	To inhibit cyclophosphamide-induced bone marrow suppression in mice	[109]
Lung protective activity			
In vivo	10–30 mg/kg, i.p.	To alleviate LPS-induced ALI mice via cGAS/STING/NF-κB signaling inhibition	[25]
In vivo	20–80 mg/kg, i.p.	To protect against airway inflammation and remodeling in ovalbumin-stimulated chronic asthma mice by controlling LAMP2, cathepsins D and S expressions	[110]
In vivo	10 mg/kg, i.p.	To attenuate bleomycin-mediated pulmonary fibrosis in mice by modulating M2 macrophage polarization via Wnt/β-catenin signaling pathway	[111]
In vitro	5 μM	To modulate pulmonary fibrosis in M2 macrophage via PI3K/Akt/β-catenin signaling pathway	[112]
Renoprotective activity			
In vitro	0.5–5 μM	To inhibit TGF-β-treated NRK-52E cells via promoting fatty acid oxidation	[23]
In vivo	5–10 mg/kg, i.g.	To prevent kidney fibrosis in mice by promoting fatty acid oxidation	[23]
Hepatoprotective activity			
In vitro	200 μM	To inhibit CCl_4-stimulated rat hepatocytes with 78% toxic recovery	[18]
Eye protective activity			
In vivo	5–10 mg/kg, i.g.	To alleviate ischemic retinopathy in mice by modulating microglia and promoting vessel integrity	[24]

significant body weight changes. This involved apoptosis, lactate dehydrogenase release, Bax/Bcl-2 regulation, and caspase-3, 8, 9 activations [32].

In patients with non-small cell lung cancer (NSCLC), immune checkpoint blockade medications, such as anti-PD-1 antibodies, exhibited encouraging antitumor activity but only a limited response. ICS-II (20–40 mg/kg, i.g.) potentiates the antitumor effects of anti-PD-1 to inhibit the tumor growth in mice bearing Lewis lung cancer (LLC) cells by decreasing chemotactic infiltration of myeloid-derived suppressor cells into the tumor microenvironment via ROS (reactive oxygen species)-mediated inactivation of SRC/ERK/STAT3 signaling pathway [33]. As shown in Fig. 4, ICS-II activated endoplasmic reticulum (ER) stress, consisting of three branches of UPR signaling, PERK, IRE1, and ATF6, and the downstream PERK/eIF2α/ATF4/CHOP pathway, enhancing apoptosis induced by cisplatin. In addition, ISC-II combined with cisplatin significantly decreased xenograft tumor growth in nude mice bearing LLC cells *in vivo* [34].

The inflammatory microenvironment, which facilitates tumor metastasis, is generated by immune cells, whereas epithelial-mesenchymal transition (EMT) plays a critical role in cancer invasion and metastasis in the inflammatory microenvironment. ICS-II could increase E-cadherin, N-cadherin, vimentin, Slug, and Snail in A549 cells [35]. It also suppressed tumor necrosis factor-α (TNF-α)-stimulated nuclear translocation of nuclear factor-kappa B (NF-κB) and phosphorylation of IκBα. It also repressed the DNA-binding

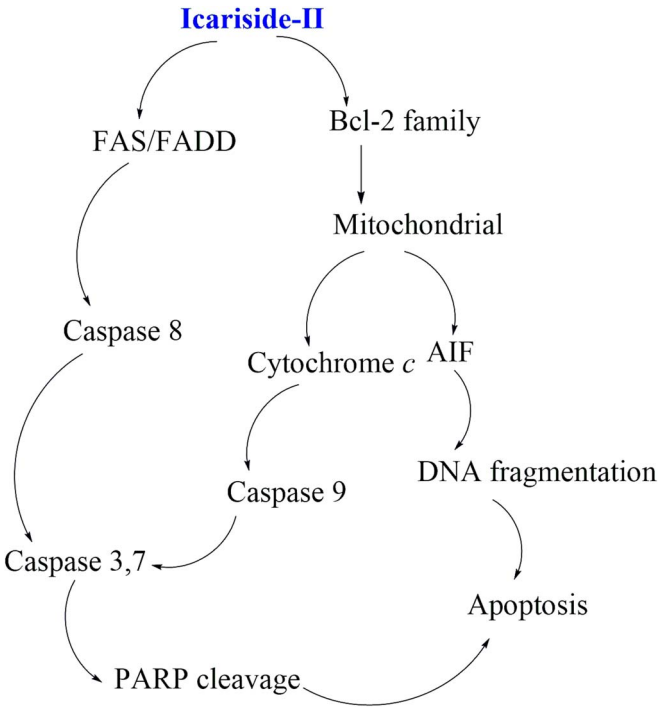

Figure 3. Cancer-related biological mechanism of icariside II on MCF7 cells.

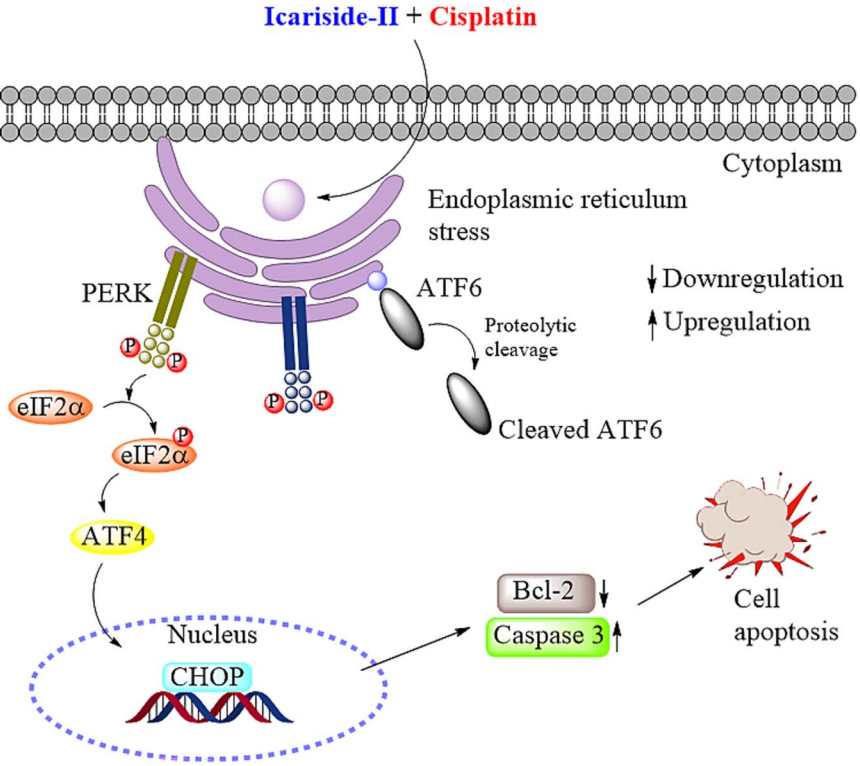

Figure 4. Cancer-related biological mechanism of icariside II + cisplatin on mice bearing LLC cells.

activity of NF-κB. Akt/GSK-3β signaling pathway is essential for ICS-II on NF-κB activation. Importantly, ICS-II hindered lung metastasis of A549 cells and EMT in mice [35].

ICS-II induced apoptosis through its anti-inflammatory effects in PC-3 prostate cancer cells [36]. This molecule suppressed arachidonic acid-induced COX-2 expression, and reduced prostaglandin E2 (PGE2) levels. In addition, it increased sub-G1 apoptotic portion, exhibited TUNEL-positive apoptotic bodies, attenuated the mitochondrial membrane potential, released cytochrome *c* into the cytosol, activated caspase-9, −8, and − 3, and cleaved PARP in PC-3 cells [36].

The abnormal energy homeostasis, which is demonstrated by a high rate of energy production (glycolysis) and energy

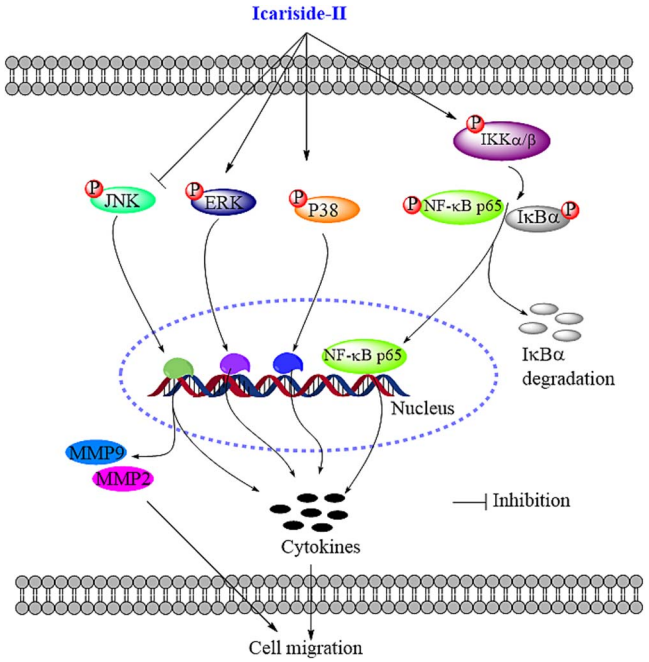

Figure 5. Cancer-related biological mechanism of icariside II on HeLa cells.

consumption (mRNA translation), is the main cause of cancer growth. ICS-II reduced glycolysis and mRNA translation in S180 fibrosarcoma cancer cells *in vitro* and mice bearing S180 cells *in vivo* due to due to suppression of mammalian target of rapamycin complex 1 (mTORC1)-eukaryotic translation initiation factor 4E-binding protein 1 (4E-BP1) axis through blocking the assembly of mTORC1 [37]. ICS-II could inhibit the tumorigenesis and growth of ovarian cancer cells *in vitro* and *in vivo* by enhancing autophagy via miR-144-3p/IGF2R axis [38]. ICS-II mainly caused ferroptosis in renal cancer cells by accumulating Fe^{2+}, malondialdehyde lipid peroxidation, and ROS via miR-324-3p/GPX4 axis regulation in both *in vivo* and *in vitro* models [39]. It is also found that the nuclear factor erythroid 2-related factor 2/antioxidant responsive element (Nrf2/ARE) is demonstrated as the underlying mechanism of ICS-II-stimulated antioxidant effects in HepG2 cells [40]. In addition, ICS-II-induced mitochondrion and lysosome-mediated apoptosis was counterbalanced by an autophagic salvage response in HepG2 cells *in vitro* and *in vivo* [41].

The effects of ICS-II on the proliferation and migration of human prostate cancer cell line DU145 can be explained by enhancing autophagy via PI3K/Akt/mTOR signaling pathway [42]. ICS-II suppressed the growth and induced apoptosis in colorectal cancer cell line SW620 *in vitro* and *in vivo* via regulation of the circβ-catenin-Wnt/β-catenin axis [43]. The most important evidence was to suppress the biogenesis of circβ-catenin via epigenetically targeting DNA methyl transferases (DNMTs) to decrease global DNA [43]. ICS-II acted as a potential anti-glioblastoma agent, suppressing cell proliferation and generating apoptosis in U87 and A172 cells via inhibiting Akt activation and potentiating Forkhead box O3a (FOXO3a) activity [44].

ICS-II suppressed cervical cancer cell migration via JNK-modulated matrix metalloproteinase-2/9 (MMP-2/9) inhibition *in vitro* and *in vivo* (Fig. 5) [45]. Osteosarcoma is one of the most common primary bone malignancies, mainly occurring in children and adolescents [46]. ICS-II reduced the cell proliferation of MG-63 and Saos-2 human osteosarcoma cells via inactivating epidermal growth factor receptor (EGFR)/mTOR signaling pathway, including EGFR, PI3K/Akt/PRAS40, Raf/MEK/ERK, and mTOR [47]. In addition, ICS-II suppressed EGF-induced activation of EGFR/mTOR signaling pathway (Fig. 6).

Metastatic melanoma is the deadliest skin cancer. At a concentration of less than 100 μM, especially at 50 μM, ICS-II mainly caused apoptosis in A431 human epidermoid carcinoma cells via EGFR signaling inhibition [48]. The treatment of 20 μM ICS-II could overcome BRAF inhibitor resistance by improving ROS generation and subsequently inducing ROS-dependent apoptosis and autophagy and downregulating microphthalmia-associated transcription factor (MITF) expression in BRAF inhibitor-resistant melanoma cells [49]. ICS-II (25–100 μM) inhibited cell proliferation and induced cell cycle arrest via ROS-p38-p35 signaling pathway in A375 human melanoma cells [50]. ICS-II (10 μM) has synergistically promoted paclitaxel (10 nM)-induced apoptosis in A375 cells by activating caspase 3 and decreasing interleukin-8 (IL-8) and VEGF via TLR4/MyD88/ERK signaling pathway [51]. In another report, ICS-II (20 μM) overcomes tumor necrosis factor-related apoptosis-inducing ligand (TRAIL) resistance of A375 cancer cells via ROS-mediated downregulation of STAT3/cFLIP signaling [52]. The studied compound at 50 mg/kg induced apoptosis in mice bearing A375 cells *in vivo* through JAK/STAT3/MAPK signaling downregulation [53].

Anti-inflammatory activity

Inflammation is one of the main causes of neurodegenerative diseases in the central nervous system. ICS-II (3–10 mg/kg, i.p.) attenuated lipopolysaccharide (LPS)-mediated neuroinflammation in mice via TLR4/MyD88/NF-κB signaling inhibition [54]. As expected, ICS-II inhibited the expressions of cytokines IL-1β, TNF-α, COX-2, TLR4, MyD88, and TRAF6, the activation of microglia and astrocyte, the degradation of IκB, and the following NF-κB activation [54]. Likewise, ICS-II (5–20 μM) inhibited LPS-induced inflammation and amyloid production in rat astrocytes by regulating IKK/IκB/NF-κB/BACE1 signaling pathway [55].

Phosphorylation of endothelial nitric oxide synthase (eNOS) established a key role in the synthesis of nitric oxide (NO) in endothelial cells, which may be related to erectile dysfunction, atherosclerosis, and other diseases. At the optimal concentration of 1.0 μM, ICS-II accelerated eNOS-Ser1177 phosphorylation in human umbilical vein endothelial cells (HUVECs) via PI3K/Akt, AMPK and protein kinase C (PKC) signaling pathways and eNOS-Thr495 dephosphorylation of HUVECs via PI3K/Akt, and PKC signaling pathways [56].

Asthma is a chronic inflammatory disease of the airways, and its symptoms include goblet cell hyperplasia, mucus hypersecretion, airway remodelling, and inflammation [57]. ICS-II (10–30 mg/kg, i.p.) could attenuate eosinophils-induced airway inflammation and remodeling in asthmatic mice and inhibited TGF-β1-induced cell growth and migration in airway smooth muscle cells (ASMCs) via NF-κB/STAT3 signaling suppression [57].

Antidiabetic activity

ICS-II showed antidiabetic activity against α-glucosidase enzyme with the IC_{50} value of 106.59 μM compared to

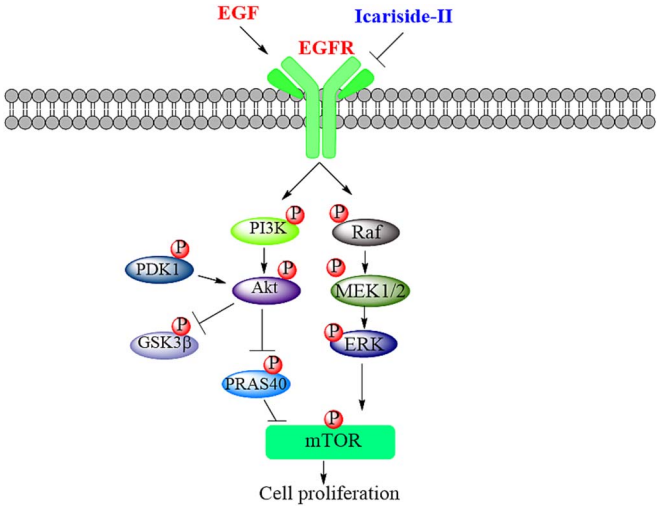

Figure 6. Cancer-related biological mechanism of icariside II on osteosarcoma cells.

that of the standard compound acarbose (IC_{50} 101.16 μM) [58]. Diabetic nephropathy, a major complication of diabetes mellitus types I and II, is a leading cause of end-stage renal disease in clinical treatments. ICS-II treatment (5 mg/kg, p.o.) could ameliorate diabetic nephropathy in STZ-induced diabetic mice by increasing endothelial cell contents and reducing oxidative stress levels via TGF-β/Smad/CTGF signaling downregulation [59].

Figure 7 illustrates the role of ICS-II on type 2 diabetic mellitus (T2DM), in which this molecule diminished hyperglycemia and hyperlipidemia in mice by targeting PPARα/γ via ROS/NF-κB/IRS1 signaling pathway, thereby leading to the reduction of inflammatory cytokines and oxidative stress, as well as alleviation of insulin resistance [17]. The treatment of ICS-II (5 mg/kg, i.p.) could improve diabetic cardiomyopathy in streptozotocin (STZ)-stimulated diabetic mice via Akt/NOS/NF-κB signaling activation [60].

Human cavernous endothelial cells (HCECs) are frequently altered pathologically due to raised high blood glucose levels linked to diabetes. ICS-II at the low 0.01–1.0 μM concentration inhibited high glucose-mediated damages in HCECs via Akt/eNOS signaling pathway [61]. Using 0.1–10 μM ICS-II could ameliorate endothelial dysfunction by regulating the MAPK pathway via miR-126/SPRED1 in HCECs exposed to a diabetic-like environment [62].

Aphrodisiac activity

In the corpus cavernosum, the penile dorsal nerve bundle neuropathy is linked to diabetic erectile dysfunction (ED). The intra-gastric treatment of ICS-II (5 mg/kg) could diminish the diabetes-related impairment of the corpus cavernosum and major pelvic ganglion neuropathy in STZ-induced diabetic mice [63]. In the same manner, Zhou et al. reported that ICS-II was able to alter the corpus cavernosum fibrous-muscular pathological structure in diabetic mice via regulating TGFβ1/Smad2/CTGF and NO-cGMP signaling pathways [64].

ICS-II (10 mg/kg, i.p.) potentiates the effects of metformin on increasing erectile function and collagen fibril/smooth muscle cell rates, reducing mitochondrial autophagy, fasting plasma glucose (FPG), hemoglobin A1c (HbA1c), and advanced glycation ends (AGEs), and improving lipid metabolism, NOS expression, cyclic guanosine monophosphates (cGMPs), testosterone, estradiol and angiotensin II in type 2 diabetic mellitus with erectile dysfunction (T2DMED) mice via PI3K/Akt/mTOR signaling pathway [65, 66]. ICS-II (5 mg/kg, i.p.) combined with insulin (2–6 units) could restore erectile function in STZ-mediated T1D rats by eliminating metabolic memory via AGEs/RAGE oxidative stress axis downregulation [67].

An inability to sustain penile erection and experience pleasure is the hallmark of sexual dysfunction, a complex medical disorder marked by upsetting disruptions in libido and sexual responsiveness. Given the vast biodiversity, several plant extracts and drug-based natural sources have long been utilized as aphrodisiacs. Treatment of 10–40 μM ICS-II could decrease testosterone production in rat Leydig cells by depleting NAD^+ and ATP levels via necrosis, but not apoptosis [68].

ICS-II could promote the differentiation of adipose-derived stem cells (ADSCs) to Schwann cells (SCs) *in vitro* and restore ED in mice *in vivo* via miR-33/GDNF/STAT3 axis regulation [69, 70]. Obesity-associated ED is a pathologic change that might be related to a deficit of the penile endogenous stem/progenitor cells. The gavage feeding of 1.5 mg/kg ICS-II to rats resulted in restoring erectile function, and preventing smooth muscle atrophy, endothelial dysfunction, and lipid accumulation, as compared with that of a non-treated group [71].

Cardiovascular activity

The intra-gastric feeding of ICS-II (4–16 mg/kg) resulted in the attenuation of myocardial fibrosis (improvements of left ventricular function and decreases of left ventricular myocardial collagen area) in mice via NF-κB and TGF-β1/Smad2 signaling inhibitions [20]. In the same model, ICS-II (8–16 mg/kg, i.g.) improved myocardial fibrosis in mice by inhibiting collagen synthesis via MMP/TIMP-1 and TGF-β1/Smad2,3/p-p38 signaling pathways [21].

Endothelial dysfunction is commonly associated with a decreased capacity for NO production and reduced NO sensitivity, demonstrating a vital role in various vascular diseases. ICS-II (1–5 μM) could attenuate palmitic acid-mediated endothelial dysfunction via SRPK1/Akt/eNOS signaling pathway [72].

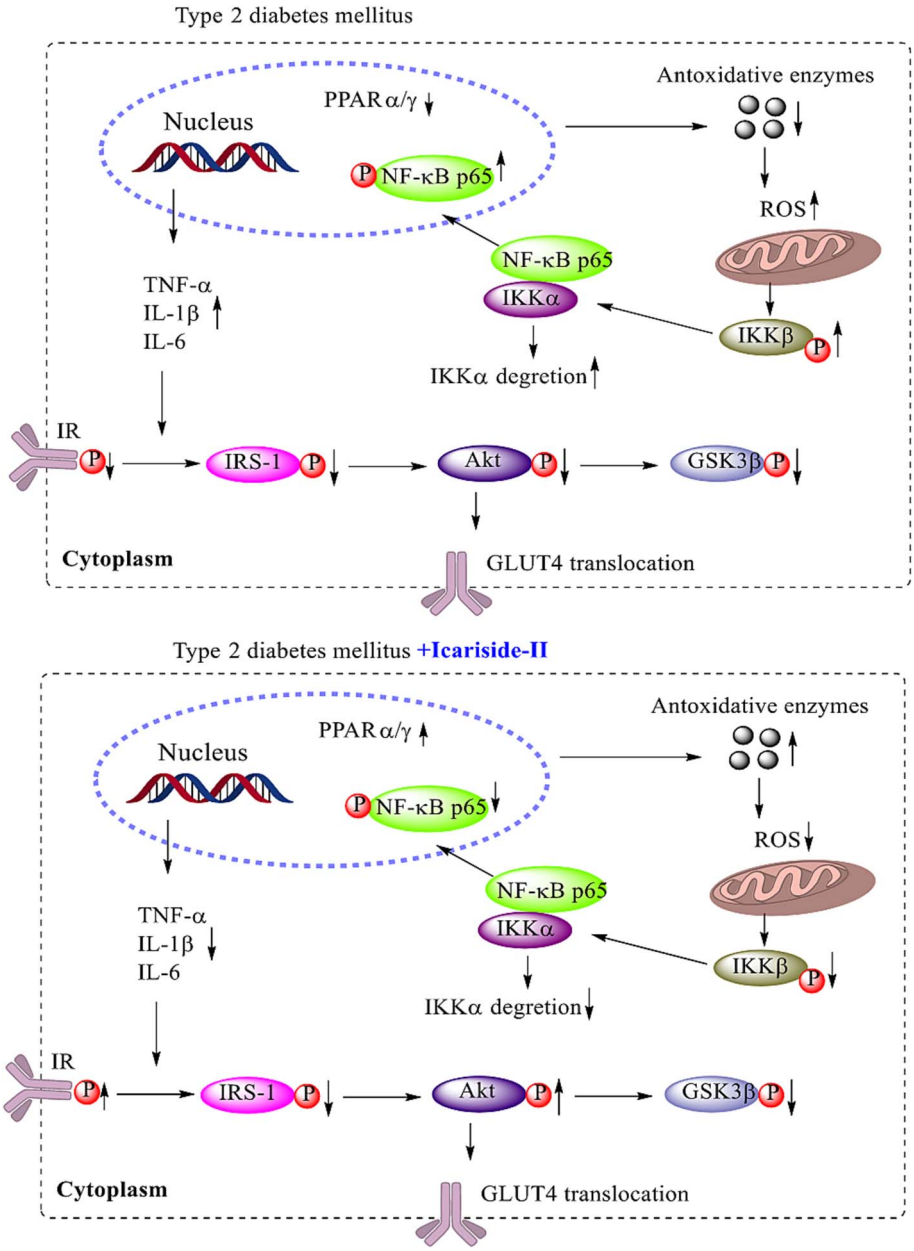

Figure 7. Antidiabetic mechanism of icariside II on mice.

Since cardiovascular illnesses begin and worsen, the basic pathophysiological change in the vascular remodeling process is represented by the phenotypic transformation of vascular smooth muscle cells (VSMCs). ICS II could restore the VSMC contractile phenotype by enhancing the focal adhesion in the rat vascular remodeling model [73]. This metabolite at 20 mg/kg, i.g., effectively attenuated the vascular remodeling process, promoted SMA-α protein expression, and inhibited osteopontin expression in mice *in vivo* [73].

Cardiac hypertrophy is associated with a shift in metabolic substrate utilization. Hence, regulating ketone body uptake and metabolism may confer protective effects against cardiac injuries [26, 74]. The *in vivo* and *in vitro* outcomes indicated that ICS-II treatment ameliorated pressure overload-induced cardiac hypertrophy and preserved heart function via apoptosis and oxidative stress reduction (Fig. 8) [75]. In addition, this metabolite inhibited excess autophagy in transverse aortic constriction (TAC)-induced hearts and angiotensin II-mediated H9C2 cardiomyocytes. Mechanistically, ICS-II regulated sirtuin expression, an activator of ketone body transportation and utilization, in cardiac remodeling [75]. Hu et al. also reported that ICS-II (2–8 μM) was able to inhibit hypoxia-mediated H9C2 cells by upregulating miR-7-5p/BTG2 axis via PI3K/Akt signaling pathway [76].

ICS-II attenuated the systolic and diastolic cardiac dysfunction and protected against hypertrophy and fibrosis in mouse hearts. The underlying mechanism may relate to the regulations of Akt, AMPkα and mTOR [77]. ICS-II (4–16 mg/kg, i.g.) could prevent hypertensive heart disease by alleviating endoplasmic reticulum stress via PERK/ATF-4/CHOP signaling pathway in hypertensive mice [78].

Myocardial infarction (MI) is the death of cardiomyocytes stimulated by insufficient energy due to myocardial ischemia and hypoxia. Meanwhile, silent mating type information

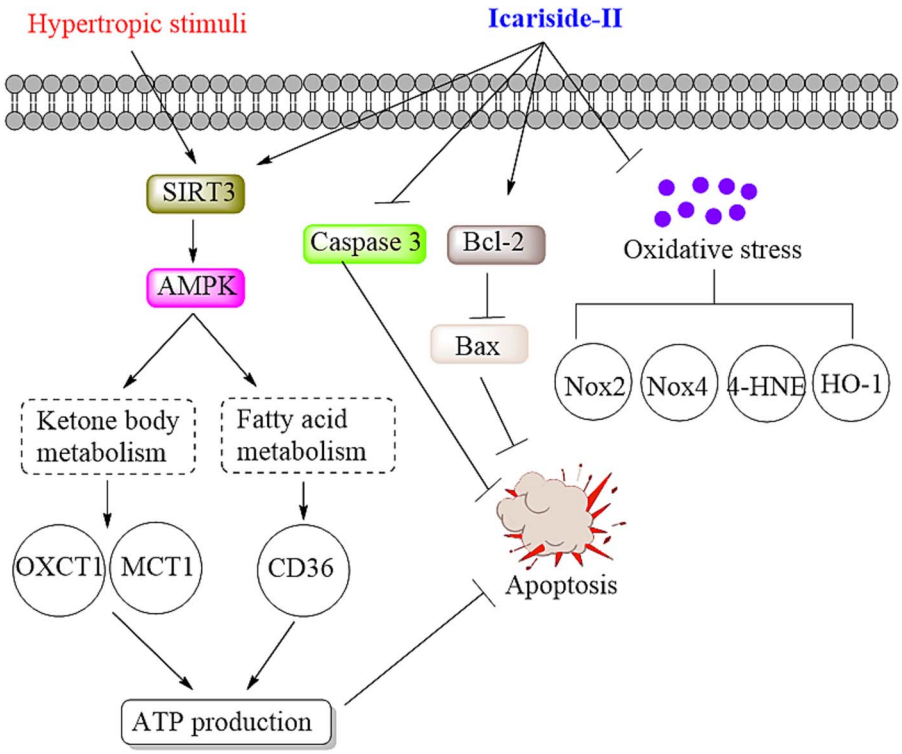

Figure 8. Cardiac hypertrophy preventing mechanism of icariside II on H9C2 cells.

regulation 2 homolog 3 (SIRT3), is essential for protecting against myocardial oxidative stress and apoptosis, which are the main MI cause [79]. ICS-II, on the one hand, mitigated MI-stimulated myocardial injuries in mice *in vivo*, on the other hand, improved H9C2 cardiomyocyte damages *in vitro* stimulated by oxygen and glucose deprivation (OGD), which were due to the inhibitions of mitochondrial oxidative stress and apoptosis [79]. Furthermore, ICS-II promoted the AMPK phosphorylation and peroxisome proliferator-activated receptor-gamma coactivator 1 alpha (PGC-1α) expression, hence activating SIRT3.[79] Li et al. also suggested that ICS-II could mitigate MI by balancing mitochondrial dynamics and decreasing oxidative stress via Nrf2/SIRT3 signaling activation *in vitro* and *in vivo* [80].

Brain protective activity

ICS-II showed selective agonist activity towards the dopamine D3 receptor with the IC_{50} value of 13.29 μM [22]. In addition, this molecule successfully mitigated MK-801-mediated schizophrenia in mice, including deficits in pre-pulse inhibition and social interaction [22]. At the optimal concentration of 3–10 μM, ICS-II promoted the differentiation of human amniotic mesenchymal stem cells into dopaminergic neuron-like cells via the PI3K signaling pathway [81]. ICS-II (10–30 mg/kg, p.o.) attenuated methamphetamine-induced neurotoxicity and behavioral impairments in mice via Keap1/Nrf2 signaling activation [82].

Cav3.2 channels have enhanced interactions with the deubiquitinase USP5, contributing to their upregulation during neuropathic pain or peripheral inflammation [83]. The treatment of 10 μM ICS-II could alleviate inflammatory and neuropathic pain in tsA-2011 cells by suppressing T-type calcium channels and USP5-Cav3.2 interactions [83]. In the *in vivo* model, this molecule suppressed either phase of the formalin-induced nocifensive responses or abolished thermal hyperalgesia in mice [83].

ICS-II (20 mg/kg, i.p.) improved cognitive deficits, ameliorated neuronal death, and reduced amyloid beta (Aβ) levels in the hippocampus [84]. This metabolite could also inhibit microglial and astrocytic activation, suppress the expressions of IL-1β, TNF-α, COX-2, and iNOS mRNA, and attenuate the Aβ-induced Bax/Bcl-2 ratio elevation and caspase-3 activation [84]. ICS-II (8–16 mg/kg, i.g.) ameliorated ibotenic acid-mediated cognitive impairment and apoptotic response through MAPK modulation in mice [85]. In this way, it protects hippocampal neurons against neurotoxicity with Bax/Bcl-2 ratio suppression, caspase-3 activation, and calbindin protein downregulation [85]. In another report, the oral administration of ICS-II (20 mg/kg) alleviated cerebral microcirculatory disturbance and improved hippocampal damage in mice after ischemia/reperfusion (I/R) [86]. The analogous results have been observed, in which this metabolite down-regulated Bax and cleaved caspase-3 expression, up-regulated Bcl-2 expression of the hippocampus, and reduced neuronal loss. In addition, it could increase the activity of complex I and decrease the MDA production [86]. Since ICS-II inhibited the Aβ synthesis in the hippocampus and cortex by increasing the expression of ADAM10 and decreasing the expression of APP and BACE1, it may be able to mitigate spatial learning and memory problems in mice [87]. Inhibition of PPARγ degradation and PERK/eIF2 phosphorylation were also involved in the course [87].

Chronic cerebral hypoperfusion (CCH) is likely to be a high-risk factor for cognitive reduction of vascular dementia, as it induces Aβ aggregation. ICS-II ameliorated cognitive impairments mediated by CCH by inhibiting the amyloidogenic pathway, which is involved in BDNF/TrkB/CREB signaling and upregulation of PPARα and PPARγ in mice [88].

The intra-gastric administration of 8 mg/kg ICS-II could also promote hippocampal neuron axon regeneration and improve learning and memory in CCH mice [89]. This mechanism was also due to the upregulation of hippocampal GAP-43 and MAP-2 protein expressions and the downregulation of Nogo-A protein expression [89].

ICS-II acted as a potential Nrf2 activator since the treatment of this metabolite (5–20 mg/kg, p.o.) provided robust neuroprotection against ischemic stroke via the astrocytic Nrf2-mediated OXPHOS/NF-κB/ferroptosis axis [90]. Cerebral I/R damage is one of the main causes of ischemic stroke. At a dose of 4–16 mg/kg, ICS-II could attenuate I/R-mediated damage in mice via PKG/GSK-3β/autophagy axis inhibition [91]. ICS-II was administered intra-gastrically at 20 mg/kg to alleviate I/R in mice via brain tissue oxidative stress reduction and Nrf2/HO-1 expression improvement [92]. The ICS-II treatment (10–30 mg/kg, i.p.) protects against I/R damage in middle cerebral artery occlusion (MCAO) mice via up-regulation of peroxisome proliferator-activated receptor α (PPARα) and PPARγ and NF-κB suppression [93]. Experimental evidence included improving neurological dysfunction, decreasing infarct volume, and inhibiting IL-1β and TGF-β1 protein expressions [93]. ICS II (16 mg/kg, i.g.) ameliorated I/R-induced blood–brain barrier disruption and neuronal apoptosis in MCAO rats by regulating the MMP9/TIMP1 balance and inhibiting the caspase 3-dependent apoptosis pathway [94]. ICS-II (1–10 mg/kg, i.g.) alleviated long-term neurocognitive deficits in mice after subarachnoid hemorrhage (SAH), reduced the development of SAH-related chronic hydrocephalus, and suppressed fibrosis via regulation of the TGF-β1/Smad/CTGF pathway [95].

A primary factor in cellular damage in many human diseases, particularly neurodegenerative illnesses, is oxidative stress. Therefore, reducing ROS production may be useful in avoiding oxidative stress-induced cell death. ICS-II acted as a phosphodiesterase 5 (PDE5) inhibitor to diminish ROS production and autophagy-stimulated by H_2O_2 in PC12 cells via ROS/GSK-3β/mitochondrial signaling pathway (Fig. 9) [96]. At the same 25–100 μM dose, ICS-II promoted neuron-like pheochromocytoma PC12 cell growth via Akt/nNOS/NO/cGMP/PKG activation [97]. The studied molecule (12.5–50 μM) alleviated oxygen–glucose deprivation/reoxygenation (OGD/R)-mediated PC12 cells oxidative damages via Nrf2/SIRT3 signaling activation [98]. The OGD/R accelerated neuronal oxidative injury and apoptosis along with reduced nucleus Nrf2, NQO-1, HO-1, and Bcl-2 protein expressions, and increased Keap1, Bax, and cleaved caspase-3 contents, whereas ICS-II remarkably reversed these changes (Fig. 10). Xu et al. also reported that ICS-II could remarkably rescue OGD/R-mediated hippocampal neuronal injury via PDE5 inhibition and PKG/CREB/BDNF/TrkB signaling activation [99]. ICS-II was reported to attenuate Aβ_{25-35}-mediated cognitive deficits via CREB/BDNF/TrkB signaling *in vitro* and *in vivo* [100]. The PDE5 inhibitor ICS-II suppressed STZ-mediated cognitive deficits in mice at 10 mg/kg [101]. Herein, this substance reduced neuronal death and Aβ_{1-40}, Aβ_{1-42} and PDE5 in the hippocampus, suppressed amyloid-beta precursor protein, BACE1, IL-1β, TNF-α, COX-2, IκBα, and NF-κB, and increased neprilysin expression [101].

At the concentration of 12.5–50 μM, ICS-II inhibited apoptosis, and oxidative stress, especially ferroptosis in the MMP^+-mediated Parkinson's disease (PD) in SK-N-SH cells, which might relate to Keap1/Nrf2/GPX4 signaling activation [102]. At the same dose, this molecule was able to protect dopaminergic neurons from 1-methyl-4-phenylpyridinium-induced neurotoxicity by downregulating histone deacetylase 2 (HDAC2) to restore mitochondrial function [103].

Bone protective activity

The optimal dose of ICS-II for improving osteogenic differentiation of bone marrow-derived stromal cells (BMSCs) was 10 μM [19]. Using 10^{-9}–10^{-5} mol/L of ICS-II could promote osteogenic differentiation of canine bone marrow mesenchymal stem cells (CBMMSCs) via PI3K/Akt/mTOR/S6K1 and MAPK/ERK signaling pathways [104, 105]. The studied flavonoid caused ALP decrease, calcium nodule formation, and enhancements of osteogenesis-related proteins Runx-2, osteocalcin, osteopontin, osterix, and basic fibroblast growth factor, especially elevation of phosphorylation levels of MAPK/ERK [105].

ICS-II at the concentration of 0.01–10 μM reciprocally stimulated osteogenesis (ALP and mineralization increases, and Runx2, Col1, and Bmp2 upregulations), and inhibited adipogenesis (Pparg, Adipsin, and Cebpb downregulations) in multipotential stromal cells (MSCs) via ERK signaling [106]. At a low concentration of 20 ng/dL, ICS-II could significantly enhance the growth and differentiation of osteoblast and osteoprotegerin expression [107]. Huang also suggested that ICS-II promoted osteoblastic, but inhibited osteoclastic differentiations with evidence being increases of ALP, OC, COL-1, and OPG, decreases of RANKL, number of multinucleated TRAP-positive cells, superoxide generation, and actin ring formation [113].

ICS-II (5 μM) significantly diminished dexamethasone-elicited apoptosis in MC3T3-E1 cells via EGFR/Akt/Nrf2 signaling pathways [108]. Herein, ICS-II activated Akt (an action in osteoblast) and Nrf2, thereby inhibiting dexamethasone-induced ROS production. Importantly, ICS-II induced heparin-binding EGF (HB-EGF) production and EGFR trans-activation [108]. EGFR inhibition, via anti-HB-EGF antibody, EGFR inhibitor AG1478 or EGFR shRNA knockdown, almost blocked ICS-II-stimulated Akt/Nrf2 activation in MC3T3-E1 cells [108].

ICS-II (10–20 mg/kg, p.o.) inhibited cyclophosphamide-induced bone marrow suppression in mice by inhibiting hematopoietic cytokines, regulating Bcl-2/Bax, and inhibiting caspase-3 expression [109]. The inhibitory effects of ICS-II on pre-osteoclast RAW 264.7 cells proliferation was enhanced by synergistic combination with icaritin at the rates of 10:1, 5:1, 1:1, 1:2, and 1: 5 [114].

Lung protective activity

One serious condition that affects the respiratory system is acute lung injury (ALI). Acute hypoxic respiratory insufficiency or respiratory failure is a series of cascade events involving inflammatory chemicals released by neutrophils, macrophages, endothelial cells, and epithelial cells during the ALI development [25]. ICS-II (10–30 mg/kg, i.g.) reduced lung histopathological damage, edema, and inflammatory cell infiltration, inflammatory cytokines in ALI mice [25]. Mechanistically, ICS II could decrease NET formation by targeting neutrophil C-X-C chemokine receptor type 4 (CXCR4), and overproduction of the NETs-related component dsDNA, hence suppressing cGAS/STING/NF-κB signaling activation [25].

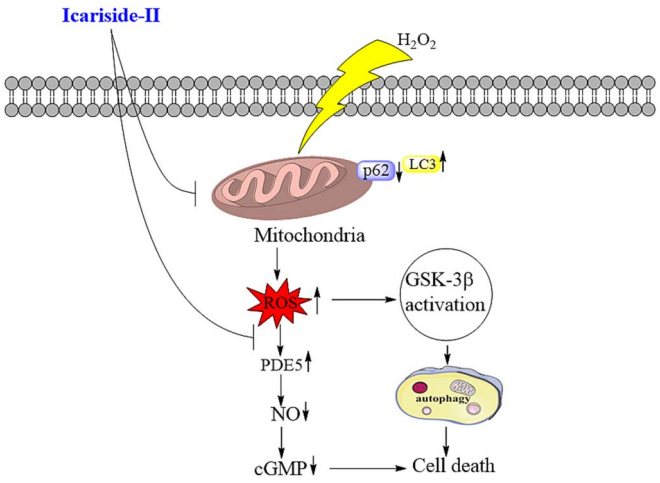

Figure 9. Neuroprotective mechanism of icariside II against H_2O_2-stimulated oxidative stress on PC12 cells.

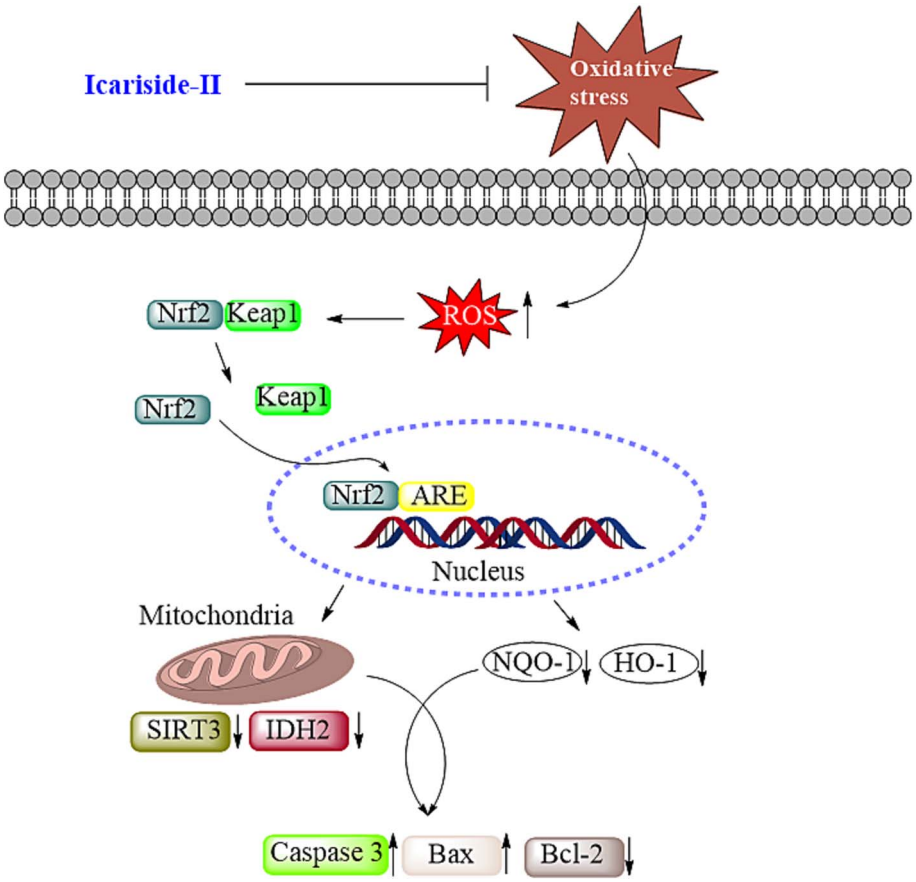

Figure 10. Neuroprotective mechanism of icariside II against OGD/R-induced oxidative stress injury on PC12 cells.

The chronic and progressive lung condition known as idiopathic pulmonary fibrosis (IPF) has an unclear cause. It is characterized by deposits of extracellular matrix, fibroblast differentiation, and recruitment and activation of immune cells. ICS-II at 20–80 mg/kg, i.p., protects against airway inflammation and remodeling by controlling lysosome-associated membrane glycoprotein 2 (LAMP2), cathepsins D and S expressions in ovalbumin-stimulated chronic asthma mice [110]. Evidence included a remarked downregulation of leukocyte count, inflammatory cytokines in bronchoalveolar lavage fluid (BALF), and peribronchial inflammation infiltration [110]. Goblet cell hyperplasia, mucus secretion, and peribronchial collagen deposition were attenuated, with the level of TGF-β and MMP-9 in BALF declining. So far, ICS-II increased Occludin and E-cadherin and decreased N-cadherin and α-smooth muscle actin (α-SMA) in lung tissues. In addition, ICS-II could decrease Beclin-1 and LC3B expressions with increasing p62 expression, thus inhibiting autophagy [110].

At 10 mg/kg, i.p., ICS-II could attenuate bleomycin-mediated IPF in mice by modulating macrophage polarization [111]. Herein, ICS-II upregulated α-SMA and collagen

production, improved lung function, decreased collagen deposition, and reduced IL-1β, TNF-α, TGF-β1, and platelet-derived growth factor (PDGF) in serum and BALF [111]. In addition, this compound attenuated the infiltration of M2 macrophages, concurrently downregulated the expression level of M2 marker genes CD206, arginase-1 (Arg-1), and chitinase-like protein 3 (YM-1) via Wnt/β-catenin signaling pathway, which modulated M2 polarization in macrophages and contributed to the amelioration of pulmonary fibrosis [111]. In the same manner, it was found that ICS-II (5 μM) significantly suppressed the proliferation of RAW264.7 cells and mitigated the pro-fibrotic characteristics of M2 macrophages, exemplified by downregulating the genes CD206, Arg-1, YM-1, and Fizz1 via PI3K/Akt/β-catenin signaling inhibition [112].

Renoprotective and hepatoprotective activities

The primary pathophysiological underpinning for the development of chronic kidney disease (CKD) is renal interstitial fibrosis (RIF). ICS-II prevented kidney fibrosis in CKD by improving lipid metabolism, fatty acid oxidation, mitochondrial function, and RIF via PPARα restoration *in vitro* and *in vivo* [23].

Hepatoprotective effects of ICS-II on CCl_4-stimulated rat hepatocytes were as potent as that of the standard compound silybin, in which it decreased the release of glutamic pyruvic transaminase, and induced 78% toxic recovery at the concentration of 200 μM [18].

Other activities

Ischemic retinopathy is classified as a vision-threatening disease that affects many people. The available therapies have drawbacks and are unable to stop the disease from getting worse. It therefore needs to have safer and more effective alternatives. In the oxygen-induced retinopathy (OIR) model, ICS-II dose-dependently reduced pathological angiogenesis and retinal hemorrhage in mice [24]. Its efficacy was deduced from GSK-3β and β-catenin regulations, which may play a critical role in inhibition of the activated microglia and exacerbation of the pathologic angiogenic process [24].

Synthetic modification

To produce derivatives with pharmacological activity enhancements, compounds ICS-II-**a**—ICS-II-**s** have been synthesized [115, 116]. Alkylation at the 7-OH position of ICS-II with dihalogenated hydrocarbons (n = 0, 1, 3, and 6) was catalyzed by K_2CO_3 to produce the corresponding intermediates in 50–65% yields. Then nucleophilic substitution between secondary amines i-iv and the halogenated hydrocarbons was finished to afford the final products II-**a**—ICS-II-**g** in 70–85% yields [115]. The remaining compounds were synthesized with a few steps in the same manner (Fig. 11) [116].

Significantly, these synthetic products were subjected to cytotoxic examinations, and the results are outlined in Table 2. In an assay against HCCLM3-LUC, HepG2, MCF-7, and MDA-MB-231 cancer cell lines, the IC_{50} values of the derivatives ICS-II-**a**—ICS-II-**g** were generally lower than those of the parent compound ICS-II (IC_{50} 21.92–39.04 μM), except for ICS-II-**e** (HCCLM3-LUC: IC_{50} 46.82 μM and MDA-MB-231: IC_{50} 31.46 μM) [115]. In the same way, the derivatives ICS-II-**i**—ICS-II-**s** possessed the IC_{50} values against MCF-7 cancer cells much lower than that of ICS-II (IC_{50} 7.52 μM). Especially, the last compound ICS-II-**s** with acetylation of all hydroxyl groups of both aglycone and glycone established the lowest IC_{50} value of 0.07 μM. Collectively, substitutions by small alkyl or heterocyclic containing nitrogenous and oxygen atoms are good strategy to enhance activity, as well as a great role of hydroxyl group of the parent molecule ICS-II in pharmacological activity.

Pharmacokinetics and bioavailability

It noted that pharmacokinetic behaviour of a phytochemical compound could be gained using the modern chromatographic techniques, especially high-performance liquid chromatography (HPLC) related analyses. The main pharmacokinetic parameters of ICS-II after intra-gastric administration of icariin to rats included the C_{max} (peak plasma concentration) of 162.4 ng/mL, T_{max} (time to peak concentration) of 1.12 h, $T_{1/2}$ (elimination half-life) of 2.08 h, $AUC_{0\text{-}t}$ (area under curve from zero to time t) of 524.6 ng.h/mL, and $AUC_{0\text{-}\infty}$ (area under curve from zero to infinity) of 532.7 ng.h/mL [117]. It noted that 91.2% of icariin was converted into ICS-II after oral administration by rats, but only 0.4% was recorded by intravenous injection [118]. The highest concentration of ICS-II in rat sera after oral administration of an *Epimedium* preparation was 14.56 nM for 60 min treatment [119]. After the oral intake of *Epimedium* purified extract, ICS-II in the plasma of healthy postmenopausal women was associated with the C_{max} of 0.74 nM, $T_{1/2}$ of 8.31 days, and $AUC_{0\text{-}\infty}$ of 8.80 nM x day [120].

After the oral administration of Chinese Xian-Xiong-Gu-Kang formula (1.5 mL of 50% EtOH extract/100 g rats), which was composed of *E. brevicornum*, *Ligusticum chuanxiong*, Radix Clematidis, *Cinnamomum cassia*, and Fructus Xanthii, to rats, ICS-II was recorded in rat plasma with C_{max} of 12.44 ng/mL, T_{max} of 0.12 h, $T_{1/2}$ of 6.13 h, and $AUC_{0\text{-}t}$ of 47.45 h.ng/mL [121]. Regarding the intake of the classical traditional Chinese medicine Xian Ling Pi San (*Epimedii Folium* and *Chuanxiong rhizoma*) to osteoarthritis rats, pharmacokinetic parameters of ICS-II included C_{max} of 63.96 ng/mL, T_{max} of 0.50 h, $T_{1/2}$ of 6.81 h, $AUC_{0\text{-}t}$ of 427.23 h.ng/mL, and $AUC_{0\text{-}\infty}$ of 465.65 h.ng/mL [122]. In the same manner, ICS-II was eliminated quickly after the oral administration of another Chinese Gushudan formula (*E. brevicornum*, *Cnidium monnieri*, *Drynaria fortune*, and *Salvia miltiorrhiza*), in which this compound was found in rat plasma with C_{max} of 102 ng/mL, T_{max} of 0.16 h, $T_{1/2}$ of 0.12 h, and $AUC_{0\text{-}\infty}$ of 16.3 h.ng/mL [123]. The oral administrations of 0.3 and 1 g/kg of Xian-Ling-Gu-Bao capsules (*E. herba*, *Dipsaci asperoidis*, Psoraleae Fructus, *Anemarrhenae rhizoma*, *S. miltiorrhizae*, and Rehmanniae Radix) resulted in the C_{max} of 0.60 and 0.83 ng/mL for ICS-II in rat plasma, respectively [124].

ICS-II was found to be metabolized to ICS-II 7-glucuronide after incubation by human liver and intestine microsomes using the UGT isoforms UGT1A1, 1A7, 1A8, 1A9, and 1A10, in which the UGT1A1 and 1A9 contributed the corresponding 25.9 and 16.0% for this process in the liver microsomes [125]. ICS-II was found to be an intermediate in forming anhydroicaritin-3-O-rha-7-O-glucoronic acid, which was detected in mice's bile, plasma, and urine [126]. *Epimedium*-derived flavonoid glycosides were metabolized rapidly by hydrolysis to ICS-II for 2 h in the rabbit intestine, but gluconolactone at the concentration of 16 mg/mL completely inhibited this process [127]. Figure 12 indicates

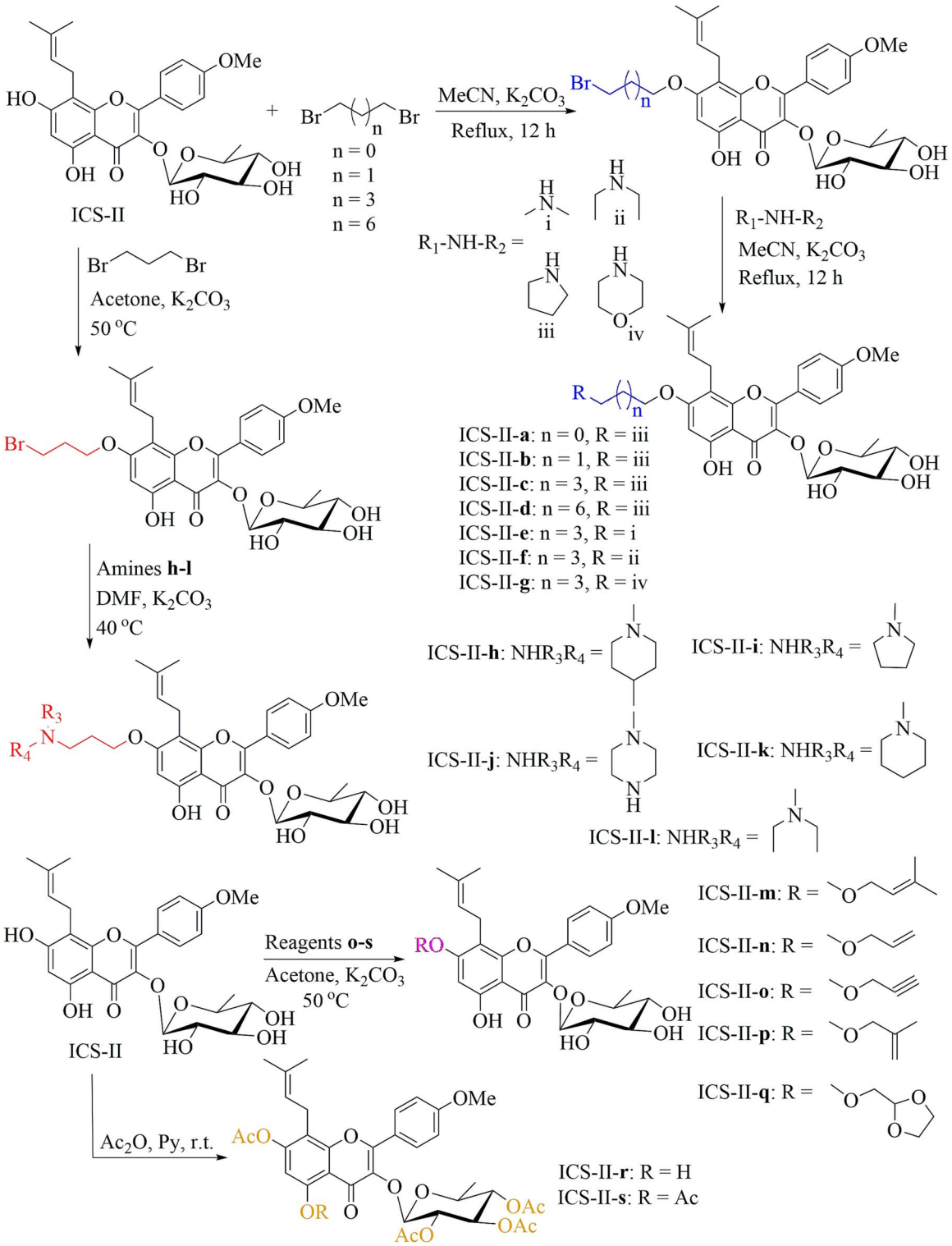

Figure 11. Synthetic steps to produce cytotoxic derivatives ICS-II-**a**—ICS-II-**s**.

the metabolic pathway of ICS-II with six derivatives M1-M6 being detected in the feces, plasma, bile, and urine [128, 129]. It was reported to contain several main steps, including desugarisation (rhamnopyranosyl removal), demethylation, oxidation (hydroxylation), glucuronidation, and glycosylation (xylopyranosyl addition).

With an efflux ratio of ICS-II decreased up to 23.5% after forming ICS-II-phospholipid complex (containing 10 μM ICS-II), phospholipid complexation can increase the intestinal absorption of ICS-II [130]. Likewise, by the presence of vitamin E tocopherol polyethylene glycol succinate 1000, the permeability coefficients (Papp) values from the apical (AP) to the basolateral (BL) of ICS-II were increased and its efflux ratios were markedly reduced in the Caco-2 cell monolayer model [131]. Using Solutol HS15 and Pluronic F127 as surfactants to develop novel mixed micelles would also enhance the oral bioavailability of ICS-II by improving the permeability and inhibiting the efflux. The efflux ratio

Table 2. Cytotoxic activity of ICS-II and its synthetic derivatives.

Compounds	Activities	References
ICS-II	$IC_{50} = 39.04\ \mu M$/HCCLM3-LUC $IC_{50} = 21.92\ \mu M$/HepG2 $IC_{50} = 30.64\ \mu M$/MCF-7[115] $IC_{50} = 7.52\ \mu M$/MCF-7[116] $IC_{50} = 32.53\ \mu M$/MDA-MB-231	[115, 116]
ICS-II-a	$IC_{50} = 18.72\ \mu M$/HCCLM3-LUC $IC_{50} = 15.41\ \mu M$/HepG2 $IC_{50} = 14.97\ \mu M$/MCF-7 $IC_{50} = 16.85\ \mu M$/MDA-MB-231	[115]
ICS-II-b	$IC_{50} = 14.23\ \mu M$/HCCLM3-LUC $IC_{50} = 7.67\ \mu M$/HepG2 $IC_{50} = 10.53\ \mu M$/MCF-7 $IC_{50} = 8.42\ \mu M$/MDA-MB-231	[115]
ICS-II-c	$IC_{50} = 13.51\ \mu M$/HCCLM3-LUC $IC_{50} = 7.67\ \mu M$/HepG2 $IC_{50} = 10.98\ \mu M$/MCF-7 $IC_{50} = 10.15\ \mu M$/MDA-MB-231	[115]
ICS-II-d	$IC_{50} = 13.90\ \mu M$/HCCLM3-LUC $IC_{50} = 7.12\ \mu M$/HepG2 $IC_{50} = 10.94\ \mu M$/MCF-7 $IC_{50} = 8.58\ \mu M$/MDA-MB-231	[115]
ICS-II-e	$IC_{50} = 46.82\ \mu M$/HCCLM3-LUC $IC_{50} = 19.92\ \mu M$/HepG2 $IC_{50} = 31.46\ \mu M$/MCF-7 $IC_{50} = 31.08\ \mu M$/MDA-MB-231	[115]
ICS-II-f	$IC_{50} = 13.28\ \mu M$/HCCLM3-LUC $IC_{50} = 3.96\ \mu M$/HepG2 $IC_{50} = 2.44\ \mu M$/MCF-7 $IC_{50} = 4.21\ \mu M$/MDA-MB-231	[115]
ICS-II-g	$IC_{50} = 15.31\ \mu M$/HCCLM3-LUC $IC_{50} = 7.14\ \mu M$/HepG2 $IC_{50} = 14.61\ \mu M$/MCF-7 $IC_{50} = 9.57\ \mu M$/MDA-MB-231	[115]
ICS-II-h	$IC_{50} = 3.17\ \mu M$/MCF-7	[116]
ICS-II-i	$IC_{50} = 3.09\ \mu M$/MCF-7	[116]
ICS-II-i	$IC_{50} = 4.07\ \mu M$/MCF-7	[116]
ICS-II-k	$IC_{50} = 3.79\ \mu M$/MCF-7	[116]
ICS-II-l	$IC_{50} = 3.26\ \mu M$/MCF-7	[116]
ICS-II-m	$IC_{50} = 2.17\ \mu M$/MCF-7	[116]
ICS-II-n	$IC_{50} = 2.89\ \mu M$/MCF-7	[116]
ICS-II-o	$IC_{50} = 2.79\ \mu M$/MCF-7	[116]
ICS-II-p	$IC_{50} = 3.97\ \mu M$/MCF-7	[116]
ICS-II-q	$IC_{50} = 6.28\ \mu M$/MCF-7	[116]
ICS-II-r	$IC_{50} = 1.54\ \mu M$/MCF-7	[116]
ICS-II-s	$IC_{50} = 0.70\ \mu M$/MCF-7	[116]

was found to be significantly reduced by 83.5%, and the relative bioavailability of the mixed micelles, compared with that of ICS-II, was 317% [132]. In addition, gastrointestinal safety also provided reliable clinical evidence for the safe use of this micelle [132]. The relative bioavailability of ICS-II in *Epimedium* flavonoid-rich extract-phospholipid complex and *Epimedium* flavonoid-rich extract-phospholipid complex nano-formula containing the stabilizers Aerosi and SDS was 401.63 and 684.70%, respectively [133]. This suggests that the nano-form would enhance oral bioavailability, which may be because it ameliorated lipophilicity and wettability [133].

Conclusions

The current research has systematically reviewed several scientific experimental results of prenylated flavone glycoside ICS-II. This molecule is among characteristic natural compounds found in medicinal plants of the genus *Epimedium*, the family Berberidaceae. By the glycosidic enzymatic catalysis, this metabolite was also obtained by transformation reactions from related flavones and flavone glycosides. The title compound ICS-II possessed a pyramid of pharmacological activities, including cancer-related biological activity, anti-inflammatory, antidiabetic, aphrodisiac, and cardiovascular activities, as well as protecting living organs brain, bones, lungs, kidneys, and eyes. Importantly, almost *in vitro* and *in vivo* pharmacological assays were explained by the underlying molecular mechanisms of action, such as the signaling pathways TLR8/MyD88/p38, SRC/ERK/-STAT3, PERK/eIF2α/ATF4/CHOP, mTORC1/4E/BP1, and PI3K/Akt/mTOR. Substitutions by small functional groups at the hydroxyl group of the flavone nucleus seem to be a good strategy to enhance cytotoxicity. Pharmacokinetic metabolism is related to desugarisation, demethylation, oxidation, glucuronidation, and glycosylation. Combined

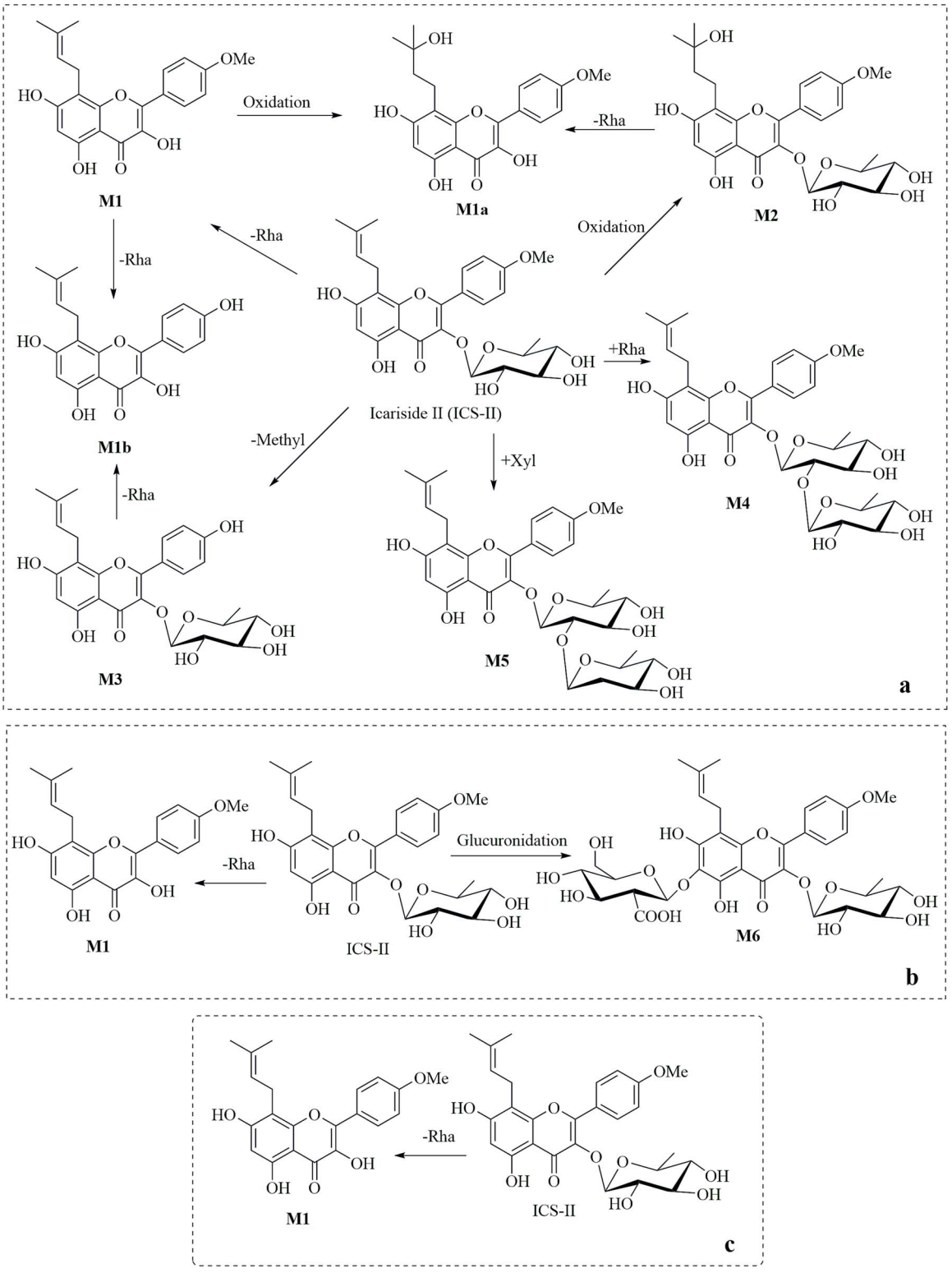

Figure 12. Metabolic pathway of icariside II in rat feces (a), plasma and bile (b), and urine (c).

nano-forms and other drugs increased the oral intake of the studied compounds.

Perspectives

ICS-II was obtained based mainly on chromatographic separations with minor amounts. Therefore, the creation of technological chemical advancement and bio-cultural approaches to yield higher rates are expected. The other types of pharmacological assays are encouraged since previous research emphasized on cancer-related biological activity, antidiabetics, sexual reproduction, cardiovascular, and the protection of the brain, lungs, and bones. In addition, preclinical and clinical considerable applications are quite limited; the principal results in pharmacological effects originated from laboratory testing. Metabolomics, molecular docking aids, and other

computational chemistry approaches are desirable to consider drug–drug interactions, half-life, and side effects, especially toxicity. More synthetic products from the parent compound ICS-II are needed. Although some commercial chemical substances enhance pharmacological and oral intake properties, combined approaches using nanoparticles, and potential drugs would be expected to produce more comparable derivatives, promoting the biological values, especially bioavailability.

List of abbreviations

Aβ: Amyloid beta; AIF: Apoptosis-induced factor; Akt: Protein kinase B; ARE: Antioxidant responsive element; BALF: Bronchoalveolar lavage fluid; BMSCs: Bone marrow-derived stromal cells; CCH: Chronic cerebral hypoperfusion; COX-2: Cyclooxygenase-2; CTGF: Connective tissue growth factor; cGMP: Cyclic guanosine monophosphate; CBMMSCs: Canine bone marrow mesenchymal stem cells; ED: Erectile dysfunction; ERK: Extracellular signal-regulated kinase; EMT: Epithelial-mesenchymal transition; EGFR: Epidermal growth factor receptor; FADD: Fas-associated death domain; FOXO3a: Forkhead box O3a; GSK-3β: Glycogen synthase kinase-3β; IC_{50}: Half maximal inhibitory concentration; HDAC2: Histone deacetylase 2; i.g.: Intra-gastric gavage; i.p.: Intraperitoneal injection; i.v.: Intravenous injection; IL-8: Interleukin-8; I/R: Ischemia/reperfusion; JAK2: Janus-activated kinase 2; LLC: Lewis lung cancer; MCAO: Middle cerebral artery occlusion; MI: Myocardial infarction; MMP-2: Metalloproteinase-2; mTOR: Mammalian target of rapamycin; MyD88: Myeloid differentiation factor 88; NF-κB: Nuclear factor-kappa B; NO: Nitric oxide; NOS: Nitric oxide synthase; Nrf2: nuclear factor erythroid 2-related factor 2; p.o.: Oral administration; PARP: Poly (ADP-ribose) polymerase; PDE5: Phosphodiesterase 5; PGE2: Prostaglandin E2; PKG: cGMP-dependent protein kinase G; PPARα: Peroxisome proliferator-activated receptor α; PI3K: Phosphoinositide 3-kinase; PD: Parkinson's disease; ROS: Reactive oxygen species; PDGF: Platelet-derived growth factor; PGC-1α: Peroxisome proliferator-activated receptor-gamma coactivator 1 alpha; α-SMA: α-Smooth muscle actin; SAH: Subarachnoid hemorrhage; STZ: Streptozotocin; SRPK1: Serine-arginine protein kinase 1; SIRT3: Silent mating type information regulation 2 homolog 3; STAT3: Signal transducer and activator of transcription 3; T2DMED: Type 2 diabetic mellitus with erectile dysfunction; TIMP-1: Tissue inhibitor of metalloproteinase-1; TRAIL: Tumor necrosis factor-related apoptosis-inducing ligand; TLR4: Toll-like receptor 4; TNF-α: Tumor necrosis factor-α; TGF-β1: Transforming growth factor-β1; VEGF Vascular endothelial growth factor.

Author contributions

L.T.H.: Conceptualization; N.T.T.: Data curation; N.N.L.: Investigation; P.T.T.N.: Resource; P.T.B.D.: Validation; V.Q.M.: Formal analysis; N.T.S.: Supervision, Writing—Review and Editing. All authors approved the final version.

Supplementary data

Supplementary data is available at *Journal of Pharmacy and Pharmacology* online.

Conflict of interest

None declared.

Funding

None declared.

Data availability

No data were used for the research described in the article.

Ethical statement

No ethical approval applies to the review due to the review of published data.

References

1. Khan MA, Kassianos AJ, Hoy WE *et al.* Promoting plant-based therapies for chronic kidney disease. *J Evid Based Integr Med* 2022;**27**:1–16. https://doi.org/10.1177/2515690X221079688
2. Linh NN, Hop NQ, Nhung PTT *et al. Glochidion* species: A review on phytochemistry and pharmacology. *Nat Prod Commun* 2024;**19**:1–30. https://doi.org/10.1177/1934578X241276962
3. Meetam T, Angspatt A, Aramwit P. Evidence of potential natural products for the management of hypertrophic scars. *J Evid Based Integr Med* 2024;**29**:1–24. https://doi.org/10.1177/2515690X241271948
4. Huong NT, Son NT. Icaritin: A phytomolecule with enormous pharmacological values. *Phytochemistry* 2023;**213**:113772. https://doi.org/10.1016/j.phytochem.2023.113772
5. Hollman PCH, Arts ICW. Flavonols, flavones and flavanols – Nature, occurrence and dietary burden. *J Sci Food Agri* 2000;**80**: 1081–93. https://doi.org/10.1002/(SICI)1097-0010(20000515)80:7<1081::AID-JSFA566>3.0.CO;2-G
6. Liu R, Li A, Sun A *et al.* Preparative isolation and purification of three flavonoids from the Chinese medicinal plant *Epimedium koreamum* Nakai by high-speed counter-current chromatography. *J Chromatograph A* 2005;**1064**:53–7. https://doi.org/10.1016/j.chroma.2004.12.026
7. Huang H, Liang M, Zhang X *et al.* Simultaneous determination of nine flavonoids and qualitative evaluation of *Herba Epimedii* by high performance liquid chromatography with ultraviolet detection. *J Sep Sci* 2007;**30**:3207–13. https://doi.org/10.1002/jssc.200700262
8. Arief ZM, Munshi AH, Shawl AS. Evaluation of medicinal value of *Epimedium elatum* on the basis of pharmacologically active constituents, icariin and Icariside-II. *Pak J Pharm Sci* 2015;**28**: 1665–9.
9. Arief ZM, Shawl AS, Munshi AH. Altitudinal variation in pharmacologically active compounds of wild and cultivated populations of *Epimedium elatum*. *J Appl Res Med Aromat Plants* 2016;**3**:48–51. https://doi.org/10.1016/j.jarmap.2016.01.001
10. Xia Q, Xu D, Huang Z *et al.* Preparation of icariside II from icariin by enzymatic hydrolysis method. *Fitoterapia* 2010;**81**: 437–42. https://doi.org/10.1016/j.fitote.2009.12.006
11. Xin X, Fan GJ, Sun Z *et al.* Biotransformation of major flavonoid glycosides in *herb Epimedii* by the fungus *Cunninghamella blakesleana*. *J Mol Catal B: Ezym* 2015;**122**:141–6. https://doi.org/10.1016/j.molcatb.2015.05.021
12. Cheng T, Yang J, Zhang T *et al.* Optimized biotransformation of icariin into icariside ii by β-glucosidase from *Trichoderma viride* using central composite design method. *Biomed Res Int* 2016;**2016**:5936947. https://doi.org/10.1155/2016/5936947
13. Han F, Kim JH, Lee IS. Microbial transformation of icariin and its derivatives. *Nat Prod Res* 2022;**36**:4103–13. https://doi.org/10.1080/14786419.2021.1975702

14. Xie J, Zhao J, Zhang N *et al.* Efficient production of isoquercitin, icariin and icariside II by a novel thermostable α-l-rhamnosidase PodoRha from *Paenibacillus odorifer* with high α-1, 6−/α-1,2-glycoside specificity. *Enyzme Microb Technol* 2022;**158**:110039. https://doi.org/10.1016/j.enzmictec.2022.110039
15. Yang L, Zhou S, Hou Y *et al.* Blue light induces biosynthesis of flavonoids in *Epimedium sagittatum* (Sieb. Et Zucc.) maxim. Leaves, a study on a light-demanding medicinal shade herb. *Ind Crop Prod* 2022;**187**:115512. https://doi.org/10.1016/j.indcrop.2022.115512
16. Huang C, Chen X, Guo B *et al.* Induction of apoptosis by icariside ii through extrinsic and intrinsic signaling pathways in human breast cancer MCF7 cells. *Biosci Biotechnol Biochem* 2012;**76**:1322–8. https://doi.org/10.1271/bbb.120077
17. Li Y, Li Y, Chen N *et al.* Icariside II exerts anti-type 2 diabetic effect by targeting PPARα/γ: Involvement of ROS/NF-κB/IRS1 signaling pathway. *Antioxidants* 2022;**11**:1706. https://doi.org/10.3390antiox11091705
18. Cho NJ, Sung SH, Lee HS *et al.* Anti-hepatotoxic activity of icariside II, a constituent of *Epimedium koreanum*. *Arch Pharm Res* 1995;**18**:289–92. https://doi.org/10.1007/BF02976415
19. Luo G, Gu F, Zhang Y *et al.* Icariside II promotes osteogenic differentiation of bone marrow stromal cells in beagle canine. *Int J Clin Exp Pathol* 2015;**8**:4367–77.
20. Shu F, Li LY, Ting WY *et al.* Icariside II attenuates myocardial fibrosis by inhibiting nuclear factor-κB and the TGF-β1/Smad2 signaling pathway in spontaneously hypertensive rats. *Biomed Pharmacol* 2018;**100**:64–71. https://doi.org/10.1016/j.biopha.2018.01.138
21. Fu S, Li Y, Wu Y *et al.* Icariside II improves myocardial fibrosis in spontaneously hypertensive rats by inhibiting collagen synthesis. *J Pharm Pharmacol* 2020;**72**:227–35. https://doi.org/10.1111/jphp.13190
22. Seong SH, Kim SH, Ryu JH *et al.* Effects of icariin and its metabolites on GPCR regulation and MK-801-induced schizophrenia-like behaviors in mice. *Molecules* 2023;**28**:7300. https://doi.org/10.3390/molecules28217300
23. Wang M, Wang J, Wang L *et al.* Icariside II prevents kidney fibrosis development in chronic kidney disease by promoting fatty acid oxidation. *Phytother Res* 2024;**38**:839–55. https://doi.org/10.1002/ptr.8085
24. Yan D, Wu Q, Li X *et al.* Icariside II alleviates ischemic retinopathy by modulating microglia and promoting vessel integrity. *J Funct Foods* 2023;**104**:105510. https://doi.org/10.1016/j.jff.2023.105510
25. Li X, Wang Y, Chen Y *et al.* Icariside II alleviates lipopolysaccharide-induced acute lung injury by inhibiting lung epithelial inflammatory and immune responses mediated by neutrophil extracellular traps. *Life Sci* 2024;**346**:122648. https://doi.org/10.1016/j.lfs.2024.122648
26. He L, Chen C, Duan S *et al.* Inhibition of estrogen sulfation by Xian-Ling-Gu-bao capsule. *J Steroid Biochem Mol Biol* 2023;**225**:106182. https://doi.org/10.1016/j.jsbmb.2022.106182
27. Lin X, Li WK, Xiao PG. Effects of icariside II from *Epimedium koreanum* on tumour cell lines in vitro. *Pharm Pharmacol Commun* 1999;**5**:701–3. https://doi.org/10.1211/146080899128734424
28. Kang SH, Jeong SJ, Kim SH *et al.* Icariside II induces apoptosis in U937 acute myeloid leukemia cells: Role of inactivation of STAT3-related signaling. *PLoS One* 2012;**7**:e28706. https://doi.org/10.1371/journal.pone.0028706
29. Kim SH, Ahn KS, Jeong SJ *et al.* Janus activated kinase 2/signal transducer and activator of transcription 3 pathway mediates icariside II-induced apoptosis in U266 multiple myeloma cells. *Eur J Pharmacol* 2011;**654**:10–6. https://doi.org/10.1016/j.ejphar.2010.11.032
30. Yang J, Lan J, Du H *et al.* Icariside II induces cell cycle arrest and differentiation via TLR8/MyD88/p38 pathway in acute myeloid leukemia cells. *Eur J Pharmacol* 2019;**846**:12–22. https://doi.org/10.1016/j.ejphar.2018.12.026
31. Kim IR, Kim YS, Yu SB *et al.* Anticancer properties of icariside II in human oral squamous cell carcinoma cells. *Int J Oral Biol* 2016;**41**:1–8. https://doi.org/10.11620/IJOB.2016.41.1.001, https://doi.org/10.11620/IJOB.2016.41.1.001
32. Song J, Huang H, Xia Z *et al.* TPGS/phospholipids mixed micelles for delivery of icariside II to multidrug-resistant breast cancer. *Integr Cancer Ther* 2016;**15**:390–9. https://doi.org/10.1177/1534735415596571
33. Kong Q, Ma M, Zhang L *et al.* Icariside II potentiates the anti-PD-1 antitumor effect by reducing chemotactic infiltration of myeloid-derived suppressor cells into the tumor microenvironment via ROS-mediated inactivation of the SRC/ERK/STAT3 signaling pathways. *Phytomedicine* 2023;**110**:154638. https://doi.org/10.1016/j.phymed.2022.154638
34. Tang Z, Du W, Xu F *et al.* Icariside II enhances cisplatin-induced apoptosis by promoting endoplasmic reticulum stress signalling in non-small cell lung cancer cells. *Int J Biol Sci* 2022;**18**:2060–74. https://doi.org/10.7150/ijbs.66630
35. Song J, Feng L, Zhong R *et al.* Icariside II inhibits the EMT of NSCLC cells in inflammatory microenvironment via down-regulation of Akt/NF-kB signaling pathway. *Mol Carcinog* 2017;**56**:36–48. https://doi.org/10.1002/mc.22471
36. Lee KS, Lee HJ, Ahn KS *et al.* Cyclooxygenase-2/prostaglandin E2 pathway medidates icariside II induced apoptosis un human PC-3 prostate cancer cells. *Cancer Lett* 2009;**280**:93–100. https://doi.org/10.1016/j.canlet.2009.02.024
37. Zhang C, Yang L, Geng YD *et al.* Icariside II, a natural mTOR inhibitor, disrupts aberrant energy homeostasis via suppressing mTORC1-4E-BP1 axis in sarcoma cells. *Oncotarget* 2016;**7**:27819–37. https://doi.org/10.18632/oncotarget.8538
38. Yuan D, Guo T, Qian H *et al.* Icariside II suppresses the tumorigenesis and development of ovarian cancer by regulating miR-144-3p/IGF2R axis. *Drug Dev Rev* 2022;**83**:1383–93. https://doi.org/10.1002/ddr.21967
39. Yui R, Zhou Y, Shi S *et al.* Icariside II induces ferroptosis in renal cell carcinoma cells by regulating the miR-324-3p/GPX4 axis. *Phytomedicine* 2022;**102**:154182. https://doi.org/10.1016/j.phymed.2022.154182
40. Gu J, Sun X, Wang G *et al.* Icariside II enhances Nrf2 nuclear translocation to upregulate phase II detoxifying enzyme expression coupled with the ERK. *Akt and JNK signaling pathways Molecules* 2011;**16**:9234–44. https://doi.org/10.3390/molecules16119234
41. Geng YD, Zhang C, Shi YM *et al.* Icariside II-induced mitochondrion and lysosome mediated apoptosis is counterbalanced by an autophagic salvage response in hepatoblastoma. *Cancer Lett* 2015;**366**:19–31. https://doi.org/10.1016/j.canlet.2015.05.032
42. Li S, Zhan Y, Xie Y *et al.* The impact of Icariside II on human prostate cancer cell proliferation, mobility, and autophagy via PI3K-AKT-mTOR signaling pathway. *Drug Des Dev Ther* 2020;**Volume 14**:4169–78. https://doi.org/10.2147/DDDT.S268524
43. Shi CJ, Li SY, Shen CH *et al.* Icariside II suppressed tumorigenesis by epigenetically regulating the circβ-catenin-Wnt/β-catenin axis in colorectal cancer. *Bioorg Chem* 2022;**124**:105800. https://doi.org/10.1016/j.bioorg.2022.105800
44. Quang K, Zhang X, Fan K *et al.* Icariside II induces cell cycle arrest and apoptosis in human glioblastoma cells through suppressing Akt activation and potentiating FOXO3a activity. *Am J Transl Res* 2017;**9**:2508–19.
45. Sun YS, Thakur K, Hu F *et al.* Icariside II suppresses cervical cancer cell migration through JNK modulated matrix metalloproteinase-2/9 inhibition *in vitro* and *in vivo*. *Biomed Pharmacother* 2020;**125**:110013. https://doi.org/10.1016/j.biopha.2020.110013

46. Huong DTL, Son NT. Pristimerin: Natural occurrence, biosynthesis, pharmacology, and pharmacokinetics. *Rev Bras* 2024;**34**:467–80. https://doi.org/10.1007/s43450-024-00520-z
47. Geng YD, Yang L, Zhang C *et al.* Blockade of epidermal growth factor receptor/mammalian target of rapamycin pathway by icariside II results in reduced cell proliferation of osteosarcoma cells. *Food Chem Toxicol* 2014;**73**:7–16. https://doi.org/10.1016/j.fct.2014.08.002
48. Wu J, Zuo F, Du J *et al.* Icariside II induces apoptosis via inhibition of the EGFR pathways in A431 human epidermoid carcinoma cells. *Mol Med Rep* 2013;**8**:597–602. https://doi.org/10.3892/mmr.2013.1557
49. Liu X, Li Z, Li M *et al.* Icariside II overcomes BRAF inhibitor resistance in melanoma by inducing ROS production and inhibiting MITF. *Oncol Rep* 2020;**44**:360–70. https://doi.org/10.3892/or.2020.7582
50. Wu J, Song T, Liu S *et al.* Icariside II inhibits cell proliferation and induces cell cycle arrest through the ROS-p38-p53 signaling pathway in A375 human melanoma cells. *Mol Med Rep* 2015;**11**:410–6. https://doi.org/10.3892/mmr.2014.2701
51. Wu J, Guan M, Wong PF *et al.* Icariside II potentiates paclitaxel-induced apoptosis in human melanoma A375 cells by inhibiting TLR4 signaling pathway. *Food Chem Toxicol* 2012;**50**:3019–24. https://doi.org/10.1016/j.fct.2012.06.027
52. Du J, Wu J, Fu X *et al.* Icariside II overcomes TRAIL resistance of melanoma cells through ROS-mediated downregulation of STAT3/cFLIP signaling. *Oncotarget* 2016;**7**:52218–29. https://doi.org/10.18632/oncotarget.10582
53. Wu J, Xu J, Eksioglu EA *et al.* Icariside II induces apoptosis of melanoma cells through the downregulation of survival pathways. *Nutr Cancer* 2013;**65**:110–7. https://doi.org/10.1080/01635581.2013.741745
54. Zhou J, Deng Y, Li F *et al.* Icariside II attenuates lipopolysaccharide-induced neuroinflammation through inhibiting TLR4/MyD88/NF-κB pathway in rats. *Biomed Pharmacol* 2019;**111**:315–24. https://doi.org/10.1016/j.biopha.2018.10.201
55. Zheng Y, Deng Y, Gao JM *et al.* Icariside II inhibits lipopolysaccharide-induced inflammation and amyloid production in rat astrocytes by regulating IKK/IκB/NF-κB/BACE1 signaling pathway. *Acta Pharmacol Sin* 2020;**41**:154–62. https://doi.org/10.1038/s41401-019-0300-2
56. Song W, Yuan Y, Tan X *et al.* Icariside II induces rapid phosphorylation of endothelial nitric oxide synthase via multiple signaling pathways. *Peer J* 2022;**10**:e1412. https://doi.org/10.7717/peerj.14192
57. Tian C, Gao F, Li X *et al.* Icariside II attenuates eosinophils-induced airway inflammation and remodeling via inactivation of NF-κB and STAT3 in an asthma mouse model. *Exp Mol Pathol* 2020;**113**:104373. https://doi.org/10.1016/j.yexmp.2020.104373
58. Kim DH, Jung HA, Sohn HS *et al.* Potential of icariin metabolites from *Epimedium koreanum* Nakai as antidiabetic therapeutic agents. *Molecules* 2017;**22**:986. https://doi.org/10.3390/molecules22060986
59. Tian W, Lei H, Guan R *et al.* Icariside II ameliorates diabetic nephropathy in streptozotocin-induced diabetic rats. *Drug Des Devel Ther* 2015;**9**:5147–57. https://doi.org/10.2147/DDDT.S90060
60. Yang L, Peng C, Xia J *et al.* Effects of icariside II ameliorates diabetic cardiomyopathy in streptozotocin-induced diabetic rats by activating Akt/NOS/NF-κB signaling. *Mol Med Rep* 2018;**17**:4099–105. https://doi.org/10.3892/mmr.2017.8342
61. Li H, Xu L, Guan R *et al.* Icariside II prevents high-glucose-induced injury on human cavernous endothelial cells through Akt-eNOS signaling pathway. *Andrology* 2015;**3**:408–16. https://doi.org/10.1111/andr.303
62. Lei H, Li H, Tian L *et al.* Icariside II ameliorates endothelial dysfunction by regulating the MAPK pathway via miR-126/SPRED1 in diabetic human cavernous endothelial cells. *Drug Des Devel Ther* 2018;**12**:1743–51. https://doi.org/10.2147/DDDT.S166734
63. Bai GY, Zhou F, Hui Y *et al.* Effects of icariside II on corpus cavernosum and major pelvic ganglion neuropathy in streptozotocin-induced diabetic rats. *Int J Mol Sci* 2014;**15**:23294–306. https://doi.org/10.3390/ijms151223294
64. Zhou F, Xin H, Liu T *et al.* Effects of icariside II on improving erectile function in rats with streptozotocin-induced diabetes. *J Andrology* 2012;**33**:832–44. https://doi.org/10.2164/jandrol.111.015172
65. Zhang J, Li S, Zhang S *et al.* Effect of Icariside II and metformin on penile erectile function, histological structure, mitochondrial autophagy, glucose-lipid metabolism, angiotensin II and sex hormone in type 2 diabetic rats with erectile dysfunction. *Sex Med* 2020;**8**:168–77. https://doi.org/10.1016/j.esxm.2020.01.006
66. Zhang J, Li S, Li S *et al.* Effect of icariside II and metformin on penile erectile function, glucose metabolism, reaction oxygen species, superoxide dismutase, and mitochondrial autophagy in type 2 diabetic rats with erectile dysfunction. *Transl Androl Urol* 2020;**9**:355–66. https://doi.org/10.21037/tau.2020.02.07
67. Wang L, Xu Y, Li H *et al.* Antioxidant icariside II combined with insulin restores erectile function in streptozotocin-induced type 1 diabetic rats. *J Cell Mol Med* 2015;**19**:960–9. https://doi.org/10.1111/jcmm.12480
68. Liu J, Li W, Piao X *et al.* Icariside II reduces testosterone production by inducing necrosis in rat Leydig cells. *J Biochem Molecular Toxicol* 2013;**27**:243–50. https://doi.org/10.1002/jbt.21481
69. Zheng T, Zhang TB, Wang CL *et al.* Icariside II promotes the differentiation of adipose tissue-derived stem cells to schwann cells to preserve erectile function after cavernous nerve injury. *Mol Cells* 2018;**41**:553–61. https://doi.org/10.14348/molcells.2018.2236
70. Zheng T, Zhang T, Zhang W *et al.* Icariside II facilitates the differentiation of ADSCs to schwann cells and restores erectile dysfunction through regulation of miR-33/GDNF axis. *Biomed Pharmacol* 2020;**125**:109888. https://doi.org/10.1016/j.biopha.2020.109888
71. Ruan Y, Lin G, Kang N *et al.* In situ activation and preservation of penile progenitor cells using icariside II in an obesity-associated erectile dysfunction rat model. *Stem Cells Develop* 2018;**27**:207–15. https://doi.org/10.1089/scd.2017.0220
72. Gu YY, Tan XH, Song WP *et al.* Icariside II attenuates palmitic acid-induced endothelial dysfunction through SRPK1-Akt-eNOS signaling pathway. *Front Pharmacol* 2022;**13**:920601. https://doi.org/10.3389/fphar.2022.920601
73. Junyaun L, Li X, Wu H *et al.* Icariside II restores vascular smooth muscle cell contractile phenotype by enhancing the focal adhesion signaling pathway in the rat vascular remodeling model. *Front Pharmacol* 2022;**13**:879615. https://doi.org/10.3389/fphar.2022.897615
74. Thoa NT, Son NT. Scutellarein: A review of chemistry and pharmacology. *J Pharm Pharmacol* 2024;**77**:352–70. https://doi.org/10.1093/jpp/rgae039
75. Han D, Wang B, Cui X *et al.* ICS II protects against cardiac hypertrophy by regulating metabolic remodelling, not by inhibiting autophagy. *J Cell Mol Med* 2021;**25**:1074–88. https://doi.org/10.1111/jcmm.16175
76. Hu D, Gu Y, Wu D *et al.* Icariside II protects cardiomyocytes from hypoxia-induced injury by upregulating the miR-7-5p/BTG2 axis and activating the PI3K/Akt signaling pathway. *Int J Mol Med* 2020;**46**:1453–65. https://doi.org/10.3892/ijmm.2020.4677
77. Liu XY, Liao HH, Feng H *et al.* Icariside II attenuates cardiac remodeling via AMPKα2/mTORC1 *in vivo* and *in vitro*. *J Pharmacol Sci* 2018;**138**:38–45. https://doi.org/10.1016/j.jphs.2018.08.010
78. Wu Y, Yue Y, Fu S *et al.* Icariside II prevents hypertensive heart disease by alleviating endoplasmic reticulum stress via the PERK/ATF-4/ CHOP signaling pathway in spontaneously

hypertensive rats. *J Pharm Pharmacol* 2019;**71**:400–7. https://doi.org/10.1111/jphp.13041
79. Li Y, Feng L, Xie D *et al.* Icariside II, a naturally occurring SIRT3 agonist, protects against myocardial infarction through the AMPK/PGC-1α/apoptosis signaling pathway. *Antioxidants* 2022;**11**:1465. https://doi.org/10.3390/antiox11081465
80. Li Y, Feng L, Xie D *et al.* Icariside II mitigates myocardial infarction by balancing mitochondrial dynamics and reducing oxidative stress through the activation of Nrf2/SIRT3 signaling pathway. *Eur J Pharmacol* 2023;**956**:175987. https://doi.org/10.1016/j.ejphar.2023.175987
81. Kuang W, Liu T, He F *et al.* Icariside II promotes the differentiation of human amniotic mesenchymal stem cells into dopaminergic neuron-like cells. *In Vitro Cell Dev Biol –Animal* 2021;**57**:457–67. https://doi.org/10.1007/s11626-021-00556-8
82. Huang J, Ding J, Wang Z *et al.* Icariside II attenuates methamphetamine-induced neurotoxicity and behavioral impairments via activating the Keap1-Nrf2 pathway. *Oxidat Med Cell Longev* 2022;**2022**:8400876. https://doi.org/10.1155/2022/8400876
83. Ali MY, Gadotti VM, Huang S *et al.* Alleviates inflammatory and neuropathic pain by inhibiting T-type calcium channels and USP5-Cav3.2 interactions. *ACS Chem Neurosci* 2023;**14**:1859–69. https://doi.org/10.1021/acschemneuro.3c00083
84. Deng Y, Long L, Wang K *et al.* Icariside II, a broad-spectrum anti-cancer agent, reverses beta-amyloid-induced cognitive impairment through reducing inflammation and apoptosis in rats. *Front Pharmacol* 2017;**8**:39. https://doi.org/10.3389/fphar.2017.00039
85. He L, Deng Y, Gao J *et al.* Icariside II ameliorates ibotenic acid-induced cognitive impairment and apoptotic response via modulation of MAPK pathway in rats. *Phytomedicine* 2018;**41**:74–81. https://doi.org/10.1016/j.phymed.2018.01.025
86. Yan BY, Pan CS, Mao XW *et al.* Icariside II improves cerebral microcirculatory disturbance and alleviates hippocampal injury in gerbils after ischemia-reperfusion. *Brain Res* 2014;**1573**:63–73. https://doi.org/10.1016/j.brainres.2014.05.023
87. Yan L, Deng Y, Gao J *et al.* Icariside II effectively reduces spatial learning and memory impairments in Alzheimer's disease model mice targeting beta-amyloid production. *Front Pharmacol* 2017;**8**:106. https://doi.org/10.3389/fphar.2017.00106
88. Yin C, Deng Y, Liu Y *et al.* Icariside II ameliorates cognitive impairments induced by chronic cerebral hypoperfusion by inhibiting the amyloidogenic pathway: Involvement of BDNF/TrkB/CREB signaling and up-regulation of PPARα and PPARγ in rats. *Front Pharmacol* 2018;**9**:1211. https://doi.org/10.3389/fphar.2018.01211
89. Liu T, He F, Yan J *et al.* Icariside II affects hippocampal neuron axon regeneration and improves learning and memory in a chronic cerebral hypoperfusion rat model. *Int J Clin Exp Pathol* 2019;**12**:826–34.
90. Gao J, Ma C, Xia D *et al.* Icariside II preconditioning evokes robust neuroprotection against ischaemic stroke, by targeting Nrf2 and the OXPHOS/NF-κB/ferroptosis pathway. *Br J Pharmacol* 2023;**180**:308–29. https://doi.org/10.1111/bph.15961
91. Gao J, Long L, Xu F *et al.* Icariside II, a phosphodiesterase 5 inhibitor, attenuates cerebral ischaemia/reperfusion injury by inhibiting glycogen synthase kinase-3β-mediated activation of autophagy. *Br J Pharmacol* 2020;**177**:1434–52. https://doi.org/10.1111/bph.14912
92. Li Y, Meng F. Effects of icariside II on brain tissue oxidative stress and Nrf2/HO-1 expression in rats with cerebral ischemiareperfusion injury. *Acta Cir Bras* 2019;**34**:e201900208. https://doi.org/10.1590/s0102-8650201900208
93. Deng Y, Xiong D, Yin C *et al.* Icariside II protects against cerebral ischemia–reperfusion injury in rats via nuclear factor-κB inhibition and peroxisome proliferator-activated receptor up-regulation. *Neurochem Int* 2016;**96**:56–61. https://doi.org/10.1016/j.neuint.2016.02.015
94. Liu MB, Wang W, Gao JM *et al.* Icariside II attenuates cerebral ischemia/reperfusion-induced blood–brain barrier dysfunction in rats via regulating the balance of MMP9/TIMP1. *Acta Pharm Sin* 2020;**41**:1547–56. https://doi.org/10.1038/s41401-020-0409-3
95. Dong C, Ming X, Ye Z *et al.* Icariside II attenuates chronic hydrocephalus in an experimental subarachnoid hemorrhage rat model. *J Pharm Pharm Sci* 2018;**21**:318–25. https://doi.org/10.18433/jpps29811
96. Gao J, Deng Y, Yin C *et al.* Icariside II, a novel phosphodiesterase 5 inhibitor, protects against H_2O_2-induced PC12 cells death by inhibiting mitochondria-mediated autophagy. *J Cell Mol Med* 2017;**21**:375–86. https://doi.org/10.1111/jcmm.12971
97. Gao J, Xu Y, Lei M *et al.* Icariside II, a PDE5 inhibitor from *Epimedium brevicornum*, promotes neuron-like pheochromocytoma PC12 cell proliferation via activating NO/cGMP/PKG pathway. *Neurochem Int* 2018;**112**:18–26. https://doi.org/10.1016/j.neuint.2017.10.015
98. Feng L, Gao J, Liu Y *et al.* Icariside II alleviates oxygen-glucose deprivation and reoxygenationinduced PC12 cell oxidative injury by activating Nrf2/SIRT3 signaling pathway. *Biomed Pharmcol* 2018;**103**:9–17. https://doi.org/10.1016/j.biopha.2018.04.005
99. Xu F, Lv C, Deng Y *et al.* Icariside II, a PDE5 inhibitor, suppresses oxygen glucose deprivation/reperfusioninduced primary hippocampal neuronal death through activating the PKG/CREB/BDNF/TrkB signaling pathway. *Front Pharmacol* 2020;**11**:523. https://doi.org/10.3389/fphar.2020.00523
100. Liu S, Li X, Gao J *et al.* Icariside II, a phosphodiesterase-5 inhibitor, attenuates beta-amyloid induced cognitive deficits via BDNF/TrkB/CREB signaling. *Cell Physiol Biochem* 2018;**49**:1010–25. https://doi.org/10.1159/000493232
101. Yin C, Deng Y, Gao J *et al.* Icariside II, a novel phosphodiesterase-5 inhibitor, attenuates streptozotocin-induced cognitive deficits in rats. *Neurosci.* 2016;**328**:69–79. https://doi.org/10.1016/j.neuroscience.2016.04.022
102. Fan W, Zhou J. Icariside II suppresses ferroptosis to protect against MPP^+-induced Parkinson's disease through Keap1/Nrf2/GPX4 signaling. *Chin J Physiol* 2023;**66**:437–45. https://doi.org/10.4103/cjop.CJOP-D-23-00107
103. Fan W, Zhou J. Icariside II protects dopaminergic neurons from 1-methyl-4-phenylpyridinium-induced neurotoxicity by downregulating HDAC2 to restore mitochondrial function. *Exp Ther Med* 2023;**27**:40. https://doi.org/10.3892/etm.2023.12328
104. Luo G, Xu B, Huang Y. Icariside II promotes the osteogenic differentiation of canine bone marrow mesenchymal stem cells via the PI3K/AKT/mTOR/S6K1 signaling pathways. *Am J Transl Res* 2017;**9**:2077–87.
105. Luo G, Xu B, Wang W *et al.* Study of the osteogenesis effect of icariside II and icaritin on canine bone marrow mesenchymal stem cells. *J Bone Miner Metab* 2018;**36**:668–78. https://doi.org/10.1007/s00774-017-0889-5
106. Zhang D, Zhao N, Wan C *et al.* Icariin and icariside II reciprocally stimulate osteogenesis and inhibit adipogenesis of multipotential stromal cells through ERK signaling. *Evid Based Complementary Altern Med* 2021;**2021**:8069930. https://doi.org/10.1155/2021/8069930
107. Wang Q, Song D, Wu D *et al.* Effect of Icariside II on the expression of OPG in mouse osteoblasts. *Bone* 2010;**47**:S404. https://doi.org/10.1016/j.bone.2010.09.193
108. Liu W, Mao L, Ji F *et al.* Icariside II activates EGFR-Akt-Nrf2 signaling and protects osteoblasts from dexamethasone. *Oncotarget* 2017;**8**:2594–603. https://doi.org/10.18632/oncotarget.13732
109. Yang X, Lang S, Li S *et al.* Preparation of icariside I and icariside II, an exploration of their protective mechanism against cyclophosphamide-induced bone marrow suppression in mice, and their regulatory effects on immune function. *Pharmazie* 2022;**77**:32–7. https://doi.org/10.1691/ph.2022.1771
110. Zhou Y, Huang X, Yu H *et al.* TMT-based quantitative proteomics revealed protective efficacy of Icariside II against airway

inflammation and remodeling via inhibiting LAMP2, CTSD and CTSS expression in OVA-induced chronic asthma mice. *Phytomedicine* 2023;**118**:154941. https://doi.org/10.1016/j.phymed.2023.154941
111. Deng L, Ouyang B, Shi H *et al.* Icariside II attenuates bleomycin-induced pulmonary fibrosis by modulating macrophage polarization. *J Ethnopharmacol* 2023;**317**:116810. https://doi.org/10.1016/j.jep.2023.116810
112. Deng L, Ouyang B, Tang W *et al.* Icariside II modulates pulmonary fibrosis via PI3K/Akt/β-catenin pathway inhibition of M2 macrophage program. *Phytomedicine* 2024;**130**:155687. https://doi.org/10.1016/j.phymed.2024.155687
113. Huang J, Yuan L, Wang X *et al.* Icaritin and its glycosides enhance osteoblastic, but suppress osteoclastic differentiation and activity in vitro. *Life Sci* 2007;**81**:832–40. https://doi.org/10.1016/j.lfs.2007.07.015
114. Liu YQ, Yang QX, Cheng MC *et al.* Synergistic inhibitory effect of Icariside II with Icaritin from *Herba Epimedii* on pre-osteoclastic RAW264.7 cell growth. *Phytomedicine* 2014;**21**:1633–7. https://doi.org/10.1016/j.phymed.2014.07.016
115. Wu T, Li T, Kang YN *et al.* Synthesis and biological evaluation of novel alkyl amine substituted icariside II derivatives as potential anticancer agents. *Molecules* 2018;**23**:2146. https://doi.org/10.3390/molecules23092146
116. Zhang L, Qin Z, Lian C *et al.* Synthesis, evaluation of anti-breast cancer activity in vitro of ICS II derivatives and summary of the structure-activity relationship. *Bioorg Med Chem* 2023;**81**:117188. https://doi.org/10.1016/j.bmc.2023.117188
117. Xu W, Zhang Y, Yang M *et al.* LC-MS/MS method for the simultaneous determination of icarrin and its major metabolites in rat plasma. *J Pharm Biomed Anal* 2007;**45**:667–72. https://doi.org/10.1016/j.jpba.2007.07.007
118. Cheng T, Zhang Y, Zhang T *et al.* Comparative pharmacokinetics study of icariin and icariside II in rats. *Molecules* 2015;**20**:21274–86. https://doi.org/10.3390/molecules201219763
119. Shen P, Wong SP, Li J *et al.* Simple and sensitive liquid chromatography–tandem mass spectrometry assay for simultaneous measurement of five *Epimedium* prenylflavonoids in rat sera. *J Chromatogr B* 2009;**877**:71–8. https://doi.org/10.1016/j.jchromb.2008.11.030
120. Yong EL, Cheong WF, Huang Z *et al.* Randomized, double-blind, placebo-controlled trial to examine the safety, pharmacokinetics and effects of *Epimedium* prenylflavonoids, on bone specific alkaline phosphatase and the osteoclast adaptor protein TRAF6 in post-menopausal women. *Phytomedicine* 2021;**91**:153680. https://doi.org/10.1016/j.phymed.2021.153680
121. Li J, Chen W, Wang Y *et al.* An LC-MS/MS method for simultaneous quantification of 11 components of Xian-Xiong-Gu-Kang in the plasma of osteoarthritic rats and pharmacokinetic analysis. *J Sep Sci* 2021;**44**:3386–97. https://doi.org/10.1002/jssc.202100132
122. Wu E, Zhang J, Chen W *et al.* Comparative pharmacokinetic study of nine bioactive components in osteoarthritis rat plasma using ultraperformance liquid chromatography–tandem mass spectrometry after single and combined oral administration of *Epimedii folium* and *chuanxiong rhizoma* extracts. *Biomed Chromatogr* 2023;**37**:e5518. https://doi.org/10.1002/bmc.5518
123. Liu M, Liu H, Lu X *et al.* Simultaneous determination of icariin, icariside II and osthole in rat plasma after oral administration of the extract of *Gushudan* (a Chinese compound formulation) by LC–MS/MS. *J Chromatogr B* 2007;**860**:113–20. https://doi.org/10.1016/j.jchromb.2007.10.019
124. Tang XY, Dai ZQ, Wu QC *et al.* Simultaneous determination of multiple components in rat plasma and pharmacokinetic studies at a pharmacodynamic dose of Xian-Ling-Gu-bao capsule by UPLC-MS/MS. *J Pharm Biomed Anal* 2020;**177**:112836. https://doi.org/10.1016/j.jpba.2019.112836
125. Yang J, Zhang B, Qin Z *et al.* Human UDP-glucuronosyltransferase 1A1, 1A7, 1A8, 1A9 and 1A10 are mainly responsible for icariside II-7-O-glucuronidation. *Int J Clin Exp Med* 2019;**12**:4960–71.
126. Zhao H, Fan M, Fan L *et al.* Liquid chromatography–tandem mass spectrometry analysis of metabolites in rats after administration of prenylflavonoids from *Epimedium*. *J Chromatogr B* 2010;**878**:1113–24. https://doi.org/10.1016/j.jchromb.2010.03.023
127. Zhi Hong Y, Ming Yan L, Yi D *et al.* Metabolism of *Epimedium*-derived flavonoid glycosides in intestinal flora of rabbits and its inhibition by gluconolactone. *Chin J Nat Med* 2011;**9**:461–5. https://doi.org/10.3724/SP.J.1009.2011.00461
128. Sun E, Fengjuan X, Qian Q *et al.* Ultra-performance liquid chromatography/quadrupole-time-of-flight mass spectrometry analysis of icariside II metabolites in rats. *Nat Prod Res* 2014;**28**:1525–9. https://doi.org/10.1080/14786419.2014.921684
129. Xu S, Yu J, Zhan J *et al.* Pharmacokinetics, tissue distribution, and metabolism study of icariin in rat. *Biomed Res Int* 2017;**2017**:4684962. https://doi.org/10.1155/2017/4684962
130. Jin X, Zhang ZH, Sun E *et al.* Preparation of icariside II-phospholipid complex and its absorption across Caco-2 cell monolayers. *Pharmazie* 2012;**67**:293–8. https://doi.org/10.1691/ph.2012.1110
131. Zhang Z, Huixia L, Jia X *et al.* Influence of vitamin E tocopherol polyethylene glycol succinate 1000 on intestinal absorption of icariside II. *Pharmazie* 2012;**67**:59–62. https://doi.org/10.1691/ph.2012.1090
132. Hou J, Wang J, Sun E *et al.* Preparation and evaluation of icariside II-loaded binary mixed micelles using solutol HS15 and pluronic F127 as carriers. *Drug Deliv* 2016;**23**:3248–56. https://doi.org/10.3109/10717544.2016.1167270
133. Pan C, Cao X, Tang L *et al.* Phospholipid complex of ICA and ICA II prepared by wet media milling for improving bioavailability. *Eur J Lipid Sci Technol* 2018;**120**:1700317. https://doi.org/10.1002/ejlt.201700317

Journal of Pharmacy and Pharmacology, 2025, 00, 1–22
https://doi.org/10.1093/jpp/rgaf065
Review